doi.org/10.26434/chemrxiv.7381025.v1

Photocatalytically Active Ladder Polymers

Anastasia Vogel, Mark forster, Liam Wilbraham, Charlotte Smith, Alexander Cowan, Martijn Zwijnenburg, Seb Sprick, Andrew I. Cooper

Submitted date: 26/11/2018 • Posted date: 26/11/2018

Citation information: Vogel, Anastasia; forster, Mark; Wilbraham, Liam; Smith, Charlotte; Cowan, Alexander; Zwijnenburg, Martijn; et al. (2018): Photocatalytically Active Ladder Polymers. ChemRxiv. Preprint.

Conjugated ladder polymers (cLaPs) are introduced as organic semiconductors for photocatalytic hydrogen evolution from water under sacrificial conditions. Starting from a linear conjugated polymer (cLiP1), two ladder polymers are synthesized via post-polymerization annulation and oxidation techniques to generate rigidified, planarized materials bearing dibenzo[b,d]thiophene (cLaP1) and dibenzo[b,d]thiophene sulfone subunits (cLaP2). The high photocatalytic activity of cLaP1 (1307 μmol h^{-1} g^{-1}) in comparison to cLaP2 (18 μmol h^{-1} g^{-1}) under broadband illumination (λ >295 nm) in presence of a hole-scavenger is attributed to a higher yield of long-lived charges (μs–ms timescale), as evidenced by transient absorption spectroscopy. Additionally, cLaP1 has a larger overpotential for proton reduction and thus an increased driving force for the evolution of hydrogen under sacrificial conditions.

File list (2)

Photocatalytically Active Ladder Polymers

Anastasia Vogel,[a] Mark Forster,[b] Liam Wilbraham,[c] Charlotte L. Smith,[a,b] Alexander Cowan,[b] Martijn A. Zwijnenburg,[c] Reiner Sebastian Sprick,[a] and Andrew I. Cooper[a,*]

[a] Department of Chemistry and Materials Innovation Factory, University of Liverpool, Liverpool, UK
[b] Department of Chemistry and Stephenson Institute for Renewable Energy, University of Liverpool, Liverpool, UK
[c] Department of Chemistry, University College London, London, UK

Abstract

Conjugated ladder polymers (cLaPs) are introduced as organic semiconductors for photocatalytic hydrogen evolution from water under sacrificial conditions. Starting from a linear conjugated polymer (cLiP1), two ladder polymers are synthesized via post-polymerization annulation and oxidation techniques to generate rigidified, planarized materials bearing dibenzo[*b*,*d*]thiophene (**cLaP1**) and dibenzo[*b*,*d*]thiophene sulfone subunits (**cLaP2**). The high photocatalytic activity of **cLaP1** (1307 μmol h^{-1} g^{-1}) in comparison to **cLaP2** (18 μmol h^{-1} g^{-1}) under broadband illumination (λ >295 nm) in presence of a hole-scavenger is attributed to a higher yield of long-lived charges (μs–ms timescale), as evidenced by transient absorption spectroscopy. Additionally, **cLaP1** has a larger overpotential for proton reduction and thus an increased driving force for the evolution of hydrogen under sacrificial conditions.

Introduction

The clean, sustainable production of hydrogen is one promising strategy for future zero-emission energy supply.[1] In this context, photocatalysis using heterogeneous semiconductors for water splitting has received much attention. Progress has been made in the application of both inorganic[2] and organic semiconductors, the latter triggered by the studies on carbon nitride,[3] which have inspired many follow-up studies.[4] The majority of studies focus on half reactions using sacrificial agents to produce either hydrogen or oxygen, but overall water-splitting systems have also been reported that produce both gases.[5] Conjugated polymer semiconductors have gained much attention recently[6] because of their synthetic modularity, the large number of monomers that are available, and the resulting tunability in physical properties. This has triggered a plethora of new types of polymer photocatalysts, including conjugated linear polymers (cLiPs)[‡],[7,8] conjugated microporous polymers (CMPs),[9–11] conjugated triazine frameworks (CTFs)[12] and covalent organic frameworks (COFs).[13,14] The modularity of these materials over a wide range of monomer building blocks allows the transfer of photocatalytically active subunits from one class of materials into another. This allows us, in principle, to build structure-property relationships where molecular effects are deconvoluted from solid state packing effects. A complication is that the efficacy of heterogeneous polymer photocatalysts depends on a large number of independent variables, including but not limited to the extent of conjugation and the light absorption cross-section,[15] the residual metal-content,[9,11] wettability,[16] thermodynamic driving forces for proton reduction,[15,17] and charge carrier life-times.[18] However, none of these variables has so far been singled out as the most dominant one: instead photocatalytic activity is a complex function of many different interrelated factors, often thwarting attempts to design better catalysts.

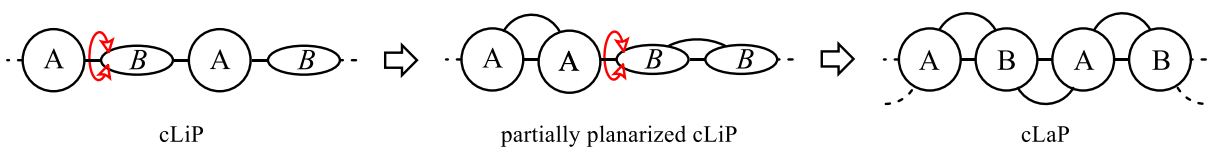

Figure 1. Graphical representation of conjugated linear polymer (cLiP) with free torsional motions, partially planarized cLiP, and conjugated ladder polymer (cLaP).

This does not mean that there are no viable structural hypotheses for polymer photocatalyst design. For example, previous studies on fluorene-type polymers suggest that partial planarization of poly(*p*-phenylene) leads to an increase in photocatalytic activity (Fig. 1).[8] Conjugated linear polymers can be further planarized forming a double-stranded polymer; that is, a so-called 'conjugated ladder polymer' (cLaP) [19–21] Ladder polymers restrict the free torsional motion between the monomer units and, in the case of cLaPs (**Figure 1**; also **BBL** and **MeLPPP**, **Figure 2**B), this leads to a fully coplanar, π-conjugated polymer backbone.[20] Thus, cLaPs tend to exhibit high thermal, optical, and mechanical stability, as well as high resistance to chemical degradation and π-conjugation, along with long exciton diffusion lengths and strong π–π stacking interactions.[19,20] In principle, all of these features are desirable in a polymer photocatalyst. Ladder polymers such as **BBL** (**Figure 2**B) have been shown to have high electron mobilities when compared to the conjugated, non-ladderized parent polymer **BBB**.[22] Also, the degree of order within the conjugated ladder polymer **MeLPPP** was highlighted to be a major contribution to its high charge carrier mobility, which resembles molecular crystals more than conventional, less ordered conjugated polymers.[23]

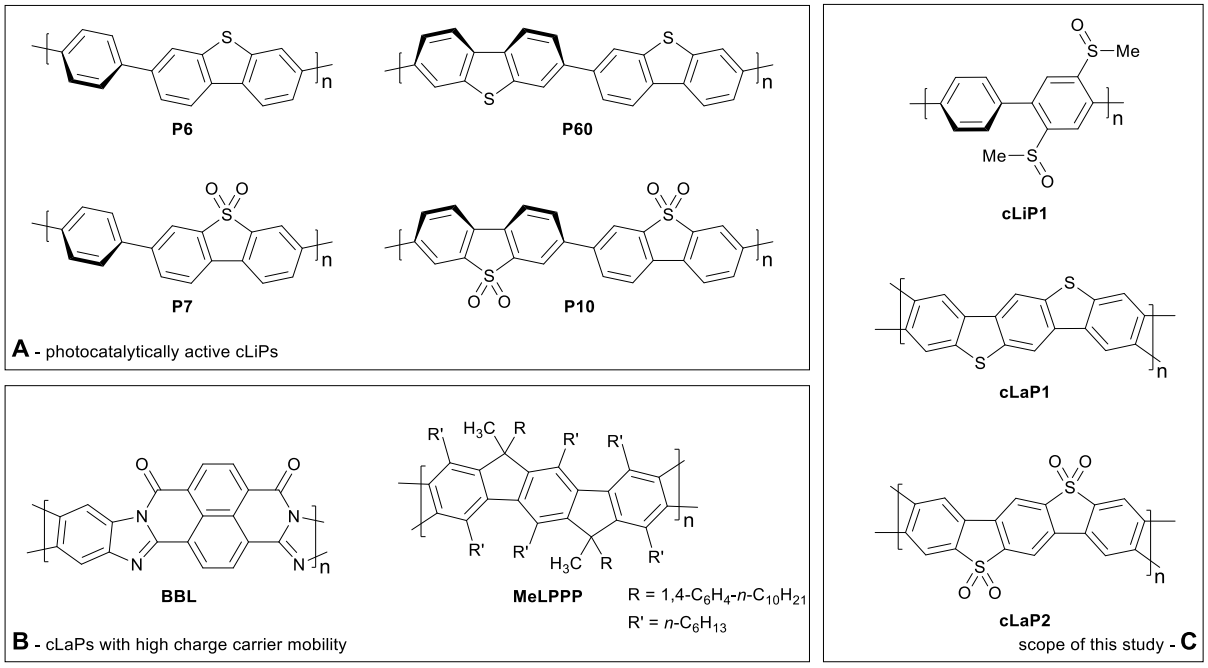

Figure 2. a) Photocatalytically active conjugated linear polymers containing dibenzo[*b*,*d*]thiophene and dibenzo[*b*,*d*]thiophene sulfone building blocks; b) Conjugated ladder polymers with reported high charge carrier mobilities; c) Scope of this study including parent linear conjugated polymer **cLiP1** and conjugated ladder polymers **cLaP1** and **cLaP2**.

Conjugated linear polymers containing dibenzo[*b*,*d*]thiophene sulfone units (as in **P7**, **Figure 2**A) have been shown repeatedly to outperform most other organic photocatalysts.[8,14,24–26] This was attributed to the co-planarization of neighbouring subunits in the polymer, increased hydrophilicity, and strong visible light absorption.[8,14] While there is one report on the use of **BBL** as a photoanode for photoelectrochemical water splitting,[27] no ladder polymers have been reported as bulk powdered photocatalysts for direct water splitting.

Here, we set out to combine structural features derived from highly active linear polymer photocatalysts with the increased conjugation that might be expected for a conjugated ladder polymer. We did this by synthesizing and analysing a series of related linear (**cLiP1**) and ladder polymers based on dibenzo[*b*,*d*]thiophene (**cLaP1**) and dibenzo[*b*,*d*]thiophene sulfone (**cLaP2**) units (**Figure 2**C), followed by testing these materials for sacrificial photocatalytic water reduction.

Results

Synthesis and Characterization

In contrast to the cross-coupling reactions (*e.g.*, Suzuki-Miyaura, Stille or Kumada coupling) that are typically used to yield linear conjugated polymers in one step, ladder polymers are usually synthesized by either (A) a single-step polycondensation reaction of tetra-functionalized building blocks or (B) polymerization and subsequent annulation of a bi-functionalized subunit to give a ladderized polymer.[20] For the synthesis of ladder polymers containing dibenzo[*b*,*d*]thiophene and dibenzo[*b*,*d*]thiophene sulfone, polymerization of an aryl bi-sulfoxide **1** via route B was chosen. Building block **1** was synthesized from 1,4-dibromobenzene (**Scheme 1**) according to literature.[28] Polymerization of **1** with 1,4-benzene diboronic acid ester via Pd(0)-catalyzed Suzuki-Miyaura cross-coupling reaction gave the parent polymer **cLiP1**.[29] Intramolecular ring-closing reaction was then performed using trifluoromethanesulfonic acid (TfOH),[29] and the intermediate polysulfonium salt (**cLaP$^+$-Me**) was dealkylated using NEt_4Br to give ladderized polymer **cLaP1**. Further oxidation of **cLaP1** with H_2O_2 in glacial acetic acid gives **cLaP2**, which is a ladder-type analogue of the linear dibenzo[*b*,*d*]thiophene sulfone polymer (**P10**).[30] $^1H\{^{13}C\}$ NMR and IR Spectra for previously reported compounds (see Experimental Section of ESI and Figures S10 and S11) agrees with literature. It is worth noting that no convenient method is available to quantify the degree of ladderization and degree of dealkylation since all materials were insoluble in common organic solvents. The total insolubility of these materials also preludes molecular weight determination.

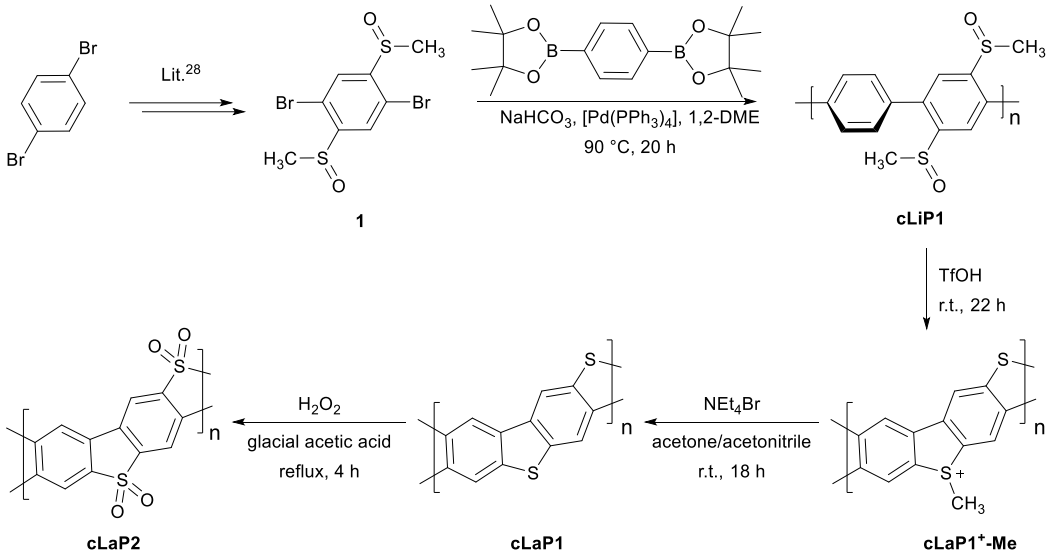

Scheme 1. Synthesis route of conjugated linear polymer **cLiP1** and related conjugated ladder polymers **cLaP1** and **cLaP2**.

Fourier-transform infrared spectroscopy (FT-IR) was used to analyze the insoluble polymers: **cLiP1** has a stretching vibration at 1032 cm^{-1} that can be attributed to the sulfoxide group ($\tilde{\nu}_{S=O}$) and, in the fingerprint region, sharp peaks (837, 747, 674 cm^{-1}) corresponding to wagging C-H and C-C vibrations for 1,4- and 1,2,4,5-substituted benzene subunits are observed (Figure S10). Upon ladderization to **cLaP1**, the spectrum is dominated by strong peaks attributed to various stretching vibrations of the triflate anion (635, 1224 cm^{-1} ($\tilde{\nu}_{C\text{-}F}$) and 1156 cm^{-1} ($\tilde{\nu}_{O=S=O}$), see also Figure S11). The fingerprint region shows a single broad peak at 832 cm^{-1} consistent with a polymer containing 1,2,4,5-substituted benzene subunits. The signals of the triflate anion (compare Figure S11, right) indicate that not all intermediate sulfonium subunits were demethylated when treated with NEt_4Br, despite further attempts to optimize the conditions. Further, the presence or absence of the sulfoxide group (1010 cm^{-1} ($\tilde{\nu}_{S=O}$)) after the ladderization could not be detected due to the overlapping signals of the triflate anion. Thus, no further conclusions on the success rate of the annulation or the presence of defects (non-annulated aryl sulfoxide groups) could be made at this point. Upon oxidation to **cLaP2**, the spectrum

shows two strong stretching vibrations (1307 cm^{-1} and 1148 cm^{-1}; symmetric and asymmetric $\tilde{\nu}_{O=S=O}$) indicating the oxidation of the dibenzo[*b*,*d*]thiophene moiety to dibenzo[*b*,*d*]thiophene dioxide (Figure S12). Additionally, no signals associated with the presence of triflate anions were observed. There is also no evidence for over-oxidation nor ring-opening reactions of the polymer to yield sulfonic acid groups.

Powder x-ray diffraction patterns (PXRD) show that polymer **cLiP1** has limited long-range order, while **cLaP1** and **cLaP2** are amorphous (Figures S17-19). Scanning electron microscopy (SEM) shows that all materials consist of *ca*. 100 nm spheres that are fused together (Figure S22). UV–Vis and photoluminescence (PL) spectroscopy were used to probe the opto-electronic properties of **cLiP1**, **cLaP1** and **cLaP2** measured as powders in the solid-state (**Figure 3** and Figures S1-9): Polymer **cLiP1** absorbs mostly in the UV region with an absorption edge around 415 nm. Upon ladderization of **cLiP1**, the absorption edge shifts by about 100 nm for **cLaP1**[§] and this clearly shows that the system has a higher degree of conjugation as the annulation of neighbouring conjugated units reduces their respective torsion angles close to zero degrees as the system is rigidified (compare Figure S38). As expected,[8] the oxidation to **cLaP2** led to only minor changes in the UV-vis spectrum. Polymer **cLiP1** has an estimated optical gap of 3.01 eV, while both ladderized polymers **cLaP1** and **cLaP2** show narrower optical gaps of 2.41 and 2.30 eV (for Tauc plots see Figures S1-5), respectively.

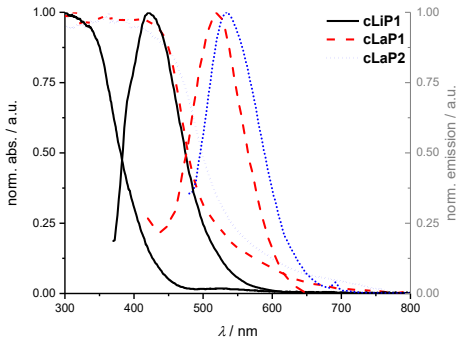

Figure 3. Normalized UV–vis absorption and photoluminescence emission spectra of **cLiP1** (black, full lines), **cLaP1** (red, dashed lines) and **cLaP2** (blue, dotted lines) from powder samples.

The fluorescence emission spectra in solid state show the same bathochromic shifts as the UV-vis absorption spectra. Moreover, a smaller Stokes' shift and resolved vibronic coupling in the excitation spectrum of **cLaP2** (and less pronounced in **cLaP1**) compared to **cLiP1** (Figures S6-9) underlines once more the increased rigidity (and symmetry) of the polymer upon ladderization. Time-resolved single photon counting (TRSPC) was used to estimate the life-time of the excited state in aqueous suspension (Figures S32-34 and Table S3). Polymer **cLiP1** has a short life-time of 0.14 ns, which is similar to **cLaP1** with 0.21 ns. The dibenzo[*b*,*d*]thiophene sulfone polymer **cLaP2** has the longest life-time of the materials studied (τ_{avg} = 1.71 ns), as observed previously.[31]

Table 1. Photophysical properties, hydrogen evolution rates and palladium content

Polymer	λ_{edge} [a] / nm	E_g^{Tauc} [b] / eV	λ_{em} [c] / nm	HER (λ >295 nm) [d] / µmol h^{-1} g^{-1}	HER (λ >420 nm) [d] / µmol h^{-1} g^{-1}	Pd content [e] / wt. %
cLiP1	415	3.01	433	15 ± 2	0[f]	0.83
cLaP1	514	2.41	520	1307 ± 26	317 ± 9	0.38
cLaP1@Pt	-	-	-	2297 ± 92	1489 ± 24	0.38 (+1 Pt)[g]
cLaP2	548	2.30	534	18 ± 1	0[f]	0.36
cLaP2@Pt	-	-	-	272 ± 10	184 ± 7	0.36 (+1 Pt)[g]
P60	454	2.68	460	1295 ± 36	641 ± 20	0.49

P60@Pt	-	-	-	1703 ± 102	213 ± 5	
P6 (Lit.[8])	448	-	456, 481	1660 ± 12	432 ± 4	0.60
P7 (Lit.[8])	459	-	477	2352 ± 76	1492 ± 32	0.38
P10 (Lit.[26])	473	-	509	-	3260 ± 164	0.40

[a] Absorption on-set determined from UV-vis reflectance measurements in the solid-state; [b] Optical gap determined from absorption spectra using the Tauc method;[32] [c] Emission peak maximum determined in the solid-state; [d] Hydrogen evolution rate determined in H_2O/TEA/MeOH irradiated with a 300 W Xe light source using suitable filters; [e] Palladium content determined via ICP-MS; [f] no hydrogen was detected with five hours of irradiation; [g] Platinum was photodeposited *in situ* onto the polymer from H_2PtCl_6.

Photocatalytic Performance

The photocatalytic activity of these materials for hydrogen evolution from water in the presence of triethylamine (TEA) as a sacrificial electron donor was studied under broad-spectrum and visible light irradiation (λ >295 nm and λ > 420 nm; **Figure 4** and **Table 1**). In addition, methanol was used in the aqueous mixture to enhance miscibility of TEA with water, and to improve wettability of the polymers.[8,33] Polymer **cLiP1** showed very limited activity (15 μmol h^{-1} g^{-1}), even compared to poly(*p*-phenylene) (232 μmol h^{-1} g^{-1}).[8] Upon ladderization to **cLaP1**, the photocatalytic activity increased dramatically to 1307 μmol h^{-1} g^{-1}. When the material was recovered and used again as a photocatalyst an increase in the hydrogen evolution rate to over 2000 μmol h^{-1} g^{-1} was observed (Figure S31). This can possibly be explained by further demethylation of the catalyst during catalysis by TEA, which reduces the doping levels of the photocatalyst and a lower effective mass for the recovered catalyst and thus higher HER per gram. This is supported by post-catalysis FT-IR measurements (Figures S14): peaks associated with the presence of the triflate counterion are no longer present, and thus a no longer charged polymer species has to be assumed after irradiation. The oxidation of **cLaP1** to **cLaP2**, led to almost total loss of activity (18 μmol h^{-1} g^{-1}).

All materials were tested as synthesized without the addition of any additional metal co-catalyst. However, it has been shown that residual palladium originating from the Suzuki-Miyaura coupling reaction can act as a co-catalyst.[9,34] Inductively coupled plasma mass spectrometry (ICP-MS) measurements show that the residual palladium content decreases from 0.83 wt. % for **cLiP1** to 0.38 and 0.36 wt. % for **cLaP1** and **cLaP2**, respectively. The lower residual palladium amount might be due to the use of trifluoromethanesulfonic acid and repeated washing of **cLaP1** after the ring-closure reaction. Similarly, the oxidation giving **cLaP2** is performed in acetic acid. The use of acids has been previously shown to decrease the residual palladium loadings of insoluble conjugated microporous polymers.[35] Finally, the photocatalytic activity of **cLaP1** was increased from 317 to 1489 μmol h^{-1} g^{-1} under visible light illumination and from 1307 to 2297 μmol h^{-1} g^{-1} under broadband illumination by *in situ* photodeposition of platinum as co-catalyst (**cLaP1@Pt**, 1 wt. %). Similarly, **cLaP2** showed a 10-fold increase in activity (from 18 to 272 μmol h^{-1} g^{-1}) under broadband illumination with platinum as co-catalyst (**cLaP2@Pt**, 1 wt. %).

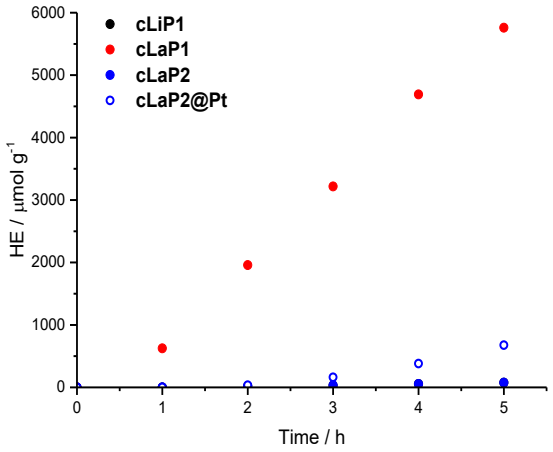

Figure 4. Hydrogen evolution of **cLiP1**, **cLaP1**and **cLaP2** from a H_2O/TEA/MeOH mixture under broadband irradiation (25 mg, 300 W Xe light source, $\lambda > 295$ nm).

Transient Absorption Spectroscopy

To try to explain the differences in catalytic activity, we studied the charge carrier life-times using transient absorption (TA) spectroscopy. TA has been shown to be an effective tool for studying the formation and life-time of electron-polaron states in polymer photocatalysts for hydrogen evolution.[26,36] Here we focus on the kinetics of species present on the µs-ms timescales following UV (355 nm) excitation of **cLiP1**, **cLaP1** and **cLaP2** in the presence of a H_2O/TEA/MeOH mixture under a nitrogen atmosphere (**Figure 5**). All three materials exhibit transient absorptions between 400-900 nm on the timescale probed, however the amplitude of the TA signal of **cLaP1** is far greater (× 5–10) than that of **cLiP1** and **cLaP2,** indicating an increase in long-lived photogenerated species. The TA spectrum of **cLaP1** contains two distinct absorptions centred at *ca.* 500 and 630 nm that decay at different rates (Figure S35 and S36, $t_{50\%}$ ~18 µs (500 nm), 25 µs (630 nm) under N_2).[§§] In the absence of methanol and TEA the long-lived TA bands at 500 and 630 nm are no longer observed (**Figure 6**). The role of TEA has previously been investigated with ultrafast TA spectroscopy[26,36] and it was shown to be required for efficient hole scavenging and for the formation of long-lived electron polarons that are suitable for proton reduction. In the absence of TEA, the excitonic states would be expected to decay rapidly after formation on timescales faster than studied here (ps-ns), in line with TCSPC measurements.[37] We therefore propose that the bands at 500 and 630 nm are due to two distinct electron populations within the sample **cLaP1**. Supporting our assignment are TA experiments carried out using oxygen as an electron scavenger. Introduction of O_2 into the system significantly decreases the TA signal at both 500 and 630 nm indicating the removal of electron populations (Figure S36). The observation of a long-lived electron signal at 630 nm for **cLaP1** is in line with a recent assignment of an electron polaron state in related dibenzo[*b,d*]thiophene sulfone linear polymers.[26] However, the assignment of both individual TA features to specific electron populations, potentially related to the presence of some residual sulfonium subunits, is challenging as the transient UV/vis spectra measured contain broad bands and our experimental resolution prevents the observation of fine structure.

Although the magnitudes of the TA signals of **cLaP2** are far smaller than **cLaP1** on the µs timescale, the kinetic traces recorded at 500 nm for **cLaP2** do indicate an extremely long-lived ($t_{50\%} = 0.3$ s) photogenerated species. The presence of extremely long-lived charges, potentially with a low thermodynamic driving force, may also be a factor behind the low HER observed for **cLaP2**. To explore this observation further, Pt was added as a co-catalyst in the hope that it may be able to either intercept photoelectrons and prevent trapping or offer suitable catalytic sites to facilitate charge transfer into solution. **cLaP2@Pt** does show an improvement in HER, increasing from 18 µmol $h^{-1}g^{-1}$ to 272 µmol $h^{-1}g^{-1}$ (**Table 1**), but a comparison of TA spectra of **cLap2** and **cLaP2@Pt** show no clear difference under nitrogen (Figure S37) suggesting the charges observed at 500 nm do not transfer to Pt

and that the hydrogen evolution catalysed with Pt happens either on a sub 10 µs timescale or that the electron population has absorption features outside of our spectral window. The addition of a Pt co-catalyst also increases the rate of hydrogen evolution in **cLap1** (**Table 1**). In this case, the increase in HER evolution following Pt addition is accompanied by a significant decrease in the TA magnitudes at both 500 and 630 nm (Figure S36) indicating that these previously long-lived charges are now transferring to Pt and on timescales faster than our experiment.

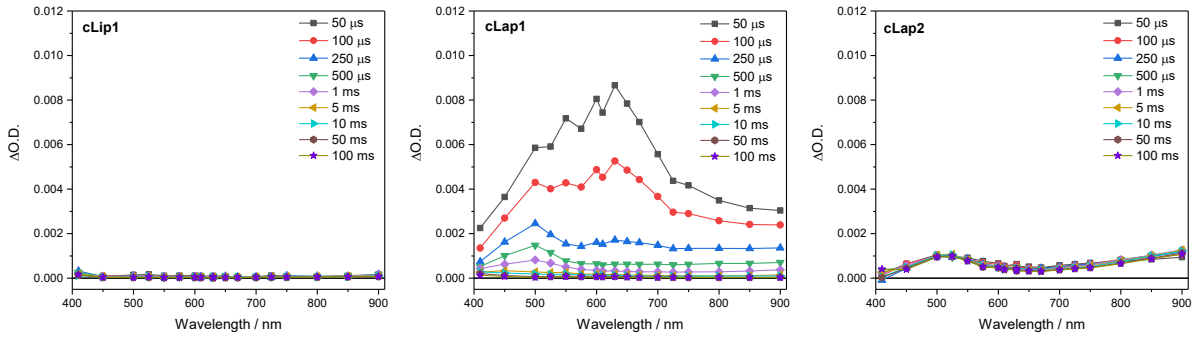

Figure 5. µs-ms TA spectra (same scale on all y-axes) of **cLiP1**, **cLaP1** and **cLaP2** suspended in H_2O/TEA/MeOH mixture following excitation with 355 nm laser (6 ns, 400 µJ cm^{-2}, 0.33 Hz). The large TA features seen with **cLaP1** correlate with the high rate of H_2 evolution.

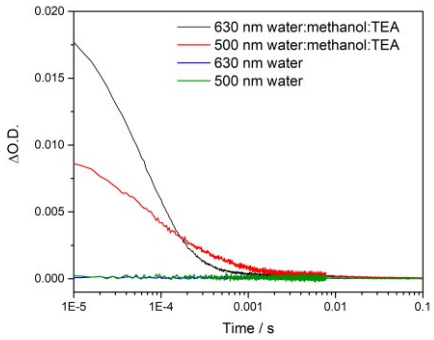

Figure 6. Kinetic traces recorded at the wavelengths indicated for **cLaP1** in either water alone or a H_2O/TEA/MeOH mixture under a nitrogen atmosphere following excitation with 355 nm (6 ns, 400 µJ cm^{-2}, 0.33 Hz) laser.

Calculations

To gain insights into the changes in thermodynamic driving forces within the investigated series of polymers, calculations were performed using a family of recently developed semi-empirical density functional tight-binding computational approaches[38] to estimate IP and EA levels as well as optical gaps for varying oligomer lengths (1-9; defined by the number of benzene bi-sulfoxide, thiophene or thiophene dioxide units, respectively). This approach, accompanied by a calibration procedure, has been shown to provide accurate optoelectronic properties with accuracy comparable to density functional theory.[39] Different oligomer lengths were tested to ensure that converged values are obtained across both ladder and non-ladder polymer species. **Figure 7** shows the calculated IP and EA values compared to the hydrogen reduction and TEA oxidation potentials at pH = 11.5. We see that each of these polymers, both ladder and non-ladder, can create charge carriers with sufficient thermodynamic driving force to drive the necessary redox chemistry required for hydrogen evolution and TEA oxidation. Both **cLaP1**/**cLiP1** are predicted to have a larger driving force for proton reduction than **cLaP2**, while **cLaP2**/**cLiP1** has a larger driving force for overall TEA oxidation to diethylamine and acetaldehyde than **cLaP1**. Assuming that overall TEA oxidation can be effectively described as a combination of two subsequent one-hole transfer-steps to TEA species in solution (I: TEA + h^+ -> TEA^+ -> TEA radical

(TEAR) + H^+ and II: TEAR + h^+ + H_2O -> diethylamine + acetaldehyde + H^+), then the exergonic first step for **cLaP2** might suggest that difference in catalytic activity may stem from differences in the driving force for proton reduction. In line with experimental UV-vis absorption spectra, ladder polymers **cLaP1** and **cLaP2** are predicted to have optical gaps that are ~1.0 and ~0.8 eV lower for **cLaP1** and **cLaP2**, respectively, than for **cLiP1** (see Table S4). Hence, **cLaP1** and **cLaP2** absorb more of the visible spectrum. The larger predicted optical gap of **cLaP1** relative to **cLaP2** (by approximately 0.1 eV) is also in line with experimental spectra.

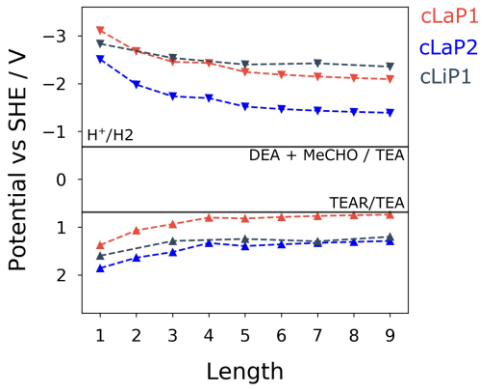

Figure 7. Calculated IP and EA (*vs* SHE) of various (ladder) polymers. IP and EA values have been computed for various oligomer lengths, where 'length' is equal to the number of aromatic rings along the polymer backbone. Hydrogen reduction and TEA oxidation potentials (pH = 11.5) are shown as horizontal lines.

Discussion

The ladder polymer **cLaP1** outperforms its non-annulated parent polymer, **cLiP1**, significantly, and the optical properties of the material after annulation show a red-shift in the absorption on-set. The ability of **cLaP1** to absorb more photons while maintaining hydrogen reduction driving force at least partially explains its higher photocatalytic activity, especially under filtered visible light. No significant changes in the optical properties were observed upon oxidation of **cLaP1** to **cLaP2**, but the resulting dibenzo[*b*,*d*]thiophene sulfone material is almost inactive. This low activity of **cLaP2** is surprising since TCSPC shows that **cLaP2** has the longest weighted average life-time of the exited state; significantly longer than **cLiP1** and **cLaP1**. Also, the introduction of dibenzo[*b*,*d*]thiophene sulfone motifs into other polymer photocatalysts has been reported to give materials with high photocatalytic activity.[8,24,25,31] However, when taking the computationally predicted band positions into account, it becomes clear that **cLaP2** has a reduced overpotential for proton reduction relative to **cLaP1** while **cLaP1** and **cLaP2** both have a reasonable driving force for TEA oxidation. From a thermodynamic perspective, **cLaP1** thus appears to be the best material in terms of combining thermodynamic driving force with light absorption. This is supported by TA measurements, which show the highest yield of long-lived charges in the case of **cLaP1**. From the TA data, it is clear that there is a direct correlation between the yield of long-lived charges present and the measured hydrogen evolution rate, suggesting that electron polaron states with lifetimes on the µs-ms timescale are required in order for hydrogen evolution to occur. This might rationalize the higher hydrogen evolution yields for **cLaP1**. The greater yield of long-lived photoelectrons may be related to more efficient hole scavenging at early timescales. The catalytic activity of the materials does not correlate with the residual palladium content, but it is unclear whether the threshold for an effect of the residual palladium on the photocatalytic performance has been reached.[9,34] Since the TA spectrum of **cLaP2** shows a persistent long-lived feature, which could be attributed to a deep-trapped charge (Figure 5, right), we loaded *in situ* **cLaP1** and **cLaP2** with a platinum co-catalyst (1 wt. %). In both cases, we observed an increase in photocatalytic performance, but there was no evidence for higher charge carrier yields in the TA spectrum of platinized **cLaP2**.

In summary, the differences in photocatalytic activity in the series of **cLiP1**, **cLaP1** and **cLaP2** can be rationalized by comparison of charge carrier life-times, light absorption, and thermodynamic driving forces. Compared with related linear polymers, such as **P6**/**P60** and **P7**/**P10** (**Figure 2**A), the idea of extending planarization across the full length of the polymer chain to enhance photocatalytic activity was not realized, at least not without the addition of a co-catalyst. For example, photocatalytic hydrogen evolution rates for unmodified **cLaP1** (1307 μmol h^{-1} g^{-1}) were found to be similar to its linear, non-ladderized analogues **P6** (1660 μmol h^{-1} g^{-1}) and **P60** (1295 μmol h^{-1} g^{-1}). However, when Pt was used as a co-catalyst, **cLaP1@Pt** outperforms **P60@Pt** under both broadband (2297 *vs*. 1703 μmol h^{-1} g^{-1}) and visible light irradiation (1489 *vs*. 213 μmol h^{-1} g^{-1}).

Conclusions

Inspired by photocatalytically active dibenzo[*b*,*d*]thiophene and dibenzo[*b*,*d*]thiophene sulfone polymers, we set out to synthesize a new class of ladderized conjugated polymer photocatalysts for photocatalytic evolution of hydrogen from water. Through post-polymerization ladderization, a planarization of the polymer chain and expansion of the π-system could be achieved, as evidenced by the bathochromic shift of the absorption edge. A significant increase in photocatalytic activity was measured for one ladder polymer (**cLaP1**) while the other (**cLaP2**) remained almost inactive. The difference in photocatalytic activity could be rationalized by analysis of charge carrier life-times via TA spectroscopy and comparison of driving forces derived from calculations. These results suggest that post-polymerization ladderization could be valuable technique in the preparation of efficient photocatalysts and that ladder polymers containing other photocatalytically active subunits might be considered for future studies.

Conflicts of interest

There are no conflicts to declare.

Acknowledgements

This project has received funding from the European Union's Horizon 2020 research and innovation programme (Marie-Skłodowska-Curie Individual Fellowship to AV) under grant agreement No 796322. The UK Engineering and Physical Sciences Research Council (EPSRC) is acknowledged for funding through grants EP/N004884/1 and EP/P034497/1. We thank Catherine M. Aitchison for help with SEM imaging.

Notes and references

‡ In the literature, both conjugated linear and conjugated ladder polymers are abbreviated as cLPs.[20] For the purposes of this paper, we will use the abbreviation cLiP for linear polymers and cLaP for ladderized polymers.

§ UV-vis and fluorescence spectra for **cLaP1** were recorded of material recovered from experiments for hydrogen evolution as this represents best the active catalysts. UV-vis spectrum of the as synthesized **cLaP1** (or rather **cLaP1^{+}-Me**) can be found in the Supporting Information.

§§ We note that the lifetimes of all bands are dependent upon the history of the sample and tend to decrease after prolonged experiments. However, the signal at 500 nm is consistently shorter lived compared to the signal at 625 nm.

1 a) P. P. Edwards, V. L. Kuznetsov, W.I.F. David and N. P. Brandon, *Energy Policy*, 2008, **36**, 4356–4362; b) S. Chu and A. Majumdar, *Nature*, 2012, **488**, 294–303; c) J. M. Ogden, *Phys. Today*, 2002, **55**, 69–75; d) A. Züttel, A. Borgschulte and L. Schlapbach, *Hydrogen as a Future Energy Carrier*, Wiley, Weinheim, 2011;

2 a) X. Chen, S. Shen, L. Guo and S. S. Mao, *Chem. Rev.*, 2010, **110**, 6503–6570; b) Z. Wang, C. Li and K. Domen, *Chem. Soc. Rev.*, 2018; c) D. Kong, Y. Zheng, M. Kobielusz, Y. Wang, Z. Bai, W. Macyk, X. Wang and J. Tang, *Mater. Today*, 2018, **21**, 897–924;

3 X. Wang, K. Maeda, A. Thomas, K. Takanabe, G. Xin, J. M. Carlsson, K. Domen and M. Antonietti, *Nat. Mater.*, 2009, **8**, 76–80.

4 a) L. Lin, Z. Yu and X. Wang, *Angew. Chem. Int. Ed.*, 2018; b) W.-J. Ong, L.-L. Tan, Y. H. Ng, S.-T. Yong and S.-P. Chai, *Chem. Rev.*, 2016, **116**, 7159–7329;

5 a) D. J. Martin, P. J. T. Reardon, S. J. A. Moniz and J. Tang, *J. Am. Chem. Soc.*, 2014, **136**, 12568–12571; b) G. Zhang, Z.-A. Lan and X. Wang, *Chem. Sci.*, 2017, **8**, 5261–5274; c) L. Lin, C. Wang, W. Ren, H. Ou, Y. Zhang and X. Wang, *Chem. Sci.*, 2017, **315**, 798; d) J. Liu, Y. Liu, N. Liu, Y. Han, X. Zhang, H. Huang, Y. Lifshitz, S.-T. Lee, J. Zhong and Z. Kang, *Science*, 2015, **347**, 970–974;

6 a) G. Zhang, Z.-A. Lan and X. Wang, *Angew. Chem. Int. Ed.*, 2016, **55**, 15712–15727; b) V. S. Vyas, V. W.-h. Lau and B. V. Lotsch, *Chem. Mater.*, 2016, **28**, 5191–5204;

7 a) C. Yang, B. C. Ma, L. Zhang, S. Lin, S. Ghasimi, K. Landfester, K. A. I. Zhang and X. Wang, *Angew. Chem. Int. Ed.*, 2016, **55**, 9202–9206; b) X. Zong, X. Miao, S. Hua, L. An, X. Gao, W. Jiang, D. Qu, Z. Zhou, X. Liu and Z. Sun, *Appl. Catal., B*, 2017, **211**, 98–105; c) L. Li, R. G. Hadt, S. Yao, W.-Y. Lo, Z. Cai, Q. Wu, B. Pandit, L. X. Chen and L. Yu, *Chem. Mater.*, 2016, **28**, 5394–5399;

8 R. S. Sprick, B. Bonillo, R. Clowes, P. Guiglion, N. J. Brownbill, B. J. Slater, F. Blanc, M. A. Zwijnenburg, D. J. Adams and A. I. Cooper, *Angew. Chem. Int. Ed.*, 2016, **55**, 1792–1796.

9 L. Li, Z. Cai, Q. Wu, W.-Y. Lo, N. Zhang, L. X. Chen and L. Yu, *J. Am. Chem. Soc.*, 2016, **138**, 7681–7686.

10 Y. Xu, C. Zhang, P. Mu, N. Mao, X. Wang, Q. He, F. Wang and J.-X. Jiang, *Sci. China Chem.*, 2017, **46**, 8574.

11 L. Li and Z. Cai, *Polym. Chem.*, 2016, **7**, 4937–4943.

12 a) K. Schwinghammer, S. Hug, M. B. Mesch, J. Senker and B. V. Lotsch, *Energy Environ. Sci.*, 2015, **8**, 3345–3353; b) S. Kuecken, A. Acharjya, L. Zhi, M. Schwarze, R. Schomäcker and A. Thomas, *Chem. Commun.*, 2017, **53**, 5854–5857; c) L. Li, W. Fang, P. Zhang, J. Bi, Y. He, J. Wang and W. Su, *J. Mater. Chem. A*, 2016, **4**, 12402–12406;

13 a) L. Stegbauer, K. Schwinghammer and B. V. Lotsch, *Chem. Sci.*, 2014, **5**, 2789–2793; b) V. S. Vyas, F. Haase, L. Stegbauer, G. Savasci, F. Podjaski, C. Ochsenfeld and B. V. Lotsch, *Nat. Commun.*, 2015, **6**, 8508;

14 X. Wang, L. Chen, S. Y. Chong, M. A. Little, Y. Wu, W.-H. Zhu, R. Clowes, Y. Yan, M. A. Zwijnenburg, R. S. Sprick and A. I. Cooper, *Nat. Chem.*, 2018.

15 R. S. Sprick, C. M. Aitchison, E. Berardo, L. Turcani, L. Wilbraham, B. M. Alston, K. E. Jelfs, M. A. Zwijnenburg and A. I. Cooper, *J. Mater. Chem. A*, 2018, **6**, 11994–12003.

16 a) R. S. Sprick, L. Wilbraham, Y. Bai, P. Guiglion, A. Monti, R. Clowes, A. I. Cooper and M. A. Zwijnenburg, *Chem. Mater.*, 2018, **30**, 5733–5742; b) Y. Wang, M. K. Bayazit, S. J. A. Moniz, Q. Ruan, C. C. Lau, N. Martsinovich and J. Tang, *Energy Environ. Sci.*, 2017, **38**, 253;

17 C. B. Meier, R. S. Sprick, A. Monti, P. Guiglion, J.-S. M. Lee, M. A. Zwijnenburg and A. I. Cooper, *Polymer*, 2017, **126**, 283–290.

18 a) O. Elbanna, M. Fujitsuka and T. Majima, *ACS Appl. Mater. Interfaces*, 2017, **9**, 34844–34854; b) R. Godin, A. Kafizas and J. R. Durrant, *Curr. Opin. Electrochem.*, 2017, **2**, 136–143;

19 U. Scherf, *J. Mater. Chem.*, 1999, **9**, 1853–1864.

20 J. Lee, A. J. Kalin, T. Yuan, M. Al-Hashimi and L. Fang, *Chem. Sci.*, 2017, **8**, 2503–2521.

21 R. G. Jones, J. Kahovec, R. Stepto, E. S. Wilks, M. Hess, T. Kitayama and W. V. Metanomski, in *Compendium of Polymer Terminology and Nomenclature: IUPAC Recommendations 2008*, ed. R. G. Jones, E. S. Wilks, W. V. Metanomski, J. Kahovec, M. Hess, R. Stepto and T. Kitayama, Royal Society of Chemistry, Cambridge, 2009, vol. 16, pp. 318–335.

22 A. Babel and S. A. Jenekhe, *J. Am. Chem. Soc.*, 2003, **125**, 13656–13657.

23 D. Hertel, U. Scherf and H. Bässler, *Adv. Mater.*, 1998, **10**, 1119–1122.

24 Z. Wang, X. Yang, T. Yang, Y. Zhao, F. Wang, Y. Chen, J. H. Zeng, C. Yan, F. Huang and J.-X. Jiang, *ACS Catal.*, 2018.

25 C. Dai, S. Xu, W. Liu, X. Gong, M. Panahandeh-Fard, Z. Liu, D. Zhang, C. Xue, K. P. Loh and B. Liu, *Small*, 2018, e1801839.

26 M. Sachs, R. S. Sprick, D. Pearce, S. A. J. Hillman, A. Monti, A. Y. Guilbert, N. J. Brownbill, S. Dimitrov, X. Shi, F. Blanc, M. A. Zwijnenburg, J. Nelson, J. R. Durrant and A. I. Cooper, *Nat. Commun.*, **2018,** accepted.
27 P. Bornoz, M. S. Prévot, X. Yu, N. Guijarro and K. Sivula, *J. Am. Chem. Soc.*, 2015, **137**, 15338–15341.
28 P. Gao, X. Feng, X. Yang, V. Enkelmann, M. Baumgarten and K. Müllen, *J. Org. Chem.*, 2008, **73**, 9207–9213.
29 A. Haryono, K. Miyatake, J. Natori and E. Tsuchida, *Macromolecules*, 1999, **32**, 3146–3149.
30 a) K. Kawabata, M. Takeguchi and H. Goto, *Macromolecules*, 2013, **46**, 2078–2091; b) M. Maisuradze, G. Phalavadishvili, N. Gakhokidze, M. Matnadze, S. Tskhvitaia and E. Kalandia, *Int. J. Org. Chem.*, 2017, **07**, 34–41; c) H. Gilman and D. L. Esmay, *J. Am. Chem. Soc.*, 1952, **74**, 2021–2024;
31 R. S. Sprick, Y. Bai, C. M. Aitchison, D. J. Woods and A. I. Cooper, *Photocatalytic Hydrogen Evolution from Water Using Heterocyclic Conjugated Microporous Polymers: Porous or Non-Porous?* DOI: 10.26434/chemrxiv.6217451.v1, accessed 14 November 2018.
32 J. Tauc, *Mater. Res. Bull.*, 1968, **3**, 37–46.
33 R. S. Sprick, B. Bonillo, M. Sachs, R. Clowes, J. R. Durrant, D. J. Adams and A. I. Cooper, *Chem. Commun.*, 2016, **52**, 10008–10011.
34 J. Kosco, M. Sachs, R. Godin, M. Kirkus, L. Francas, M. Bidwell, M. Qureshi, D. Anjum, J. R. Durrant and I. McCulloch, *Adv. Energy Mater.*, 2018, **18**, 1802181.
35 F. Wang, J. Mielby, F. H. Richter, G. Wang, G. Prieto, T. Kasama, C. Weidenthaler, H.-J. Bongard, S. Kegnæs, A. Fürstner and F. Schüth, *Angew. Chem. Int. Ed.*, 2014, **53**, 8645–8648.
36 D. J. Woods, R. S. Sprick, C. L. Smith, A. J. Cowan and A. I. Cooper, *Adv. Energy Mater.*, 2017, **7**, 1700479.
37 X. Weng, Y. Kostoulas, P. M. Fauchet, J. A. Osaheni and S. A. Jenekhe, *Phys. Rev. B*, 1995, **51**, 6838–6841.
38 a) S. Grimme, C. Bannwarth and P. Shushkov, *J. Chem. Theory Comput.*, 2017, **13**, 1989–2009; b) V. Ásgeirsson, C. A. Bauer and S. Grimme, *Chem. Sci.*, 2017, **8**, 4879–4895; c) S. Grimme and C. Bannwarth, *J. Chem. Phys.*, 2016, **145**, 54103;
39 a) L. Wilbraham, E. Berardo, L. Turcani, K. E. Jelfs and M. A. Zwijnenburg, *J. Chem. Inf. Model.*, 2018, Article ASAP, DOI: 10.1021/acs.jcim.8b00256; b) I. Heath-Apostolopoulos, L. Wilbraham and M. Zwijnenburg, *Computational High-Throughput Screening of Polymeric Photocatalysts: Exploring the Effect of Composition, Sequence Isomerism and Conformational Degrees of Freedom*. DOI:10.26434/chemrxiv.7314929.v3, accessed 14 November 2018;

Supporting Information

for

Photocatalytically Active Ladder Polymers

Anastasia Vogel,[a] Mark Forster,[c] Liam Willbram,[b] Charlotte L. Smith,[a,c] Alexander Cowan,[c] Martijn A. Zwijnenburg,[b] Reiner Sebastian Sprick,[a] and Andrew I. Cooper[a,*]

Table of Contents

1 Experimental Section

Materials and methods:

All reagents and dry solvents were obtained from Sigma-Aldrich or from TCI and used as received. 1,4-Dibromo-2,5-bis(methylsulfinyl)benzene (**1**) was synthesized according to a previously published procedure.[1] Water for the hydrogen evolution experiments was purified using an ELGA LabWater system with a Purelab Option S filtration and ion exchange column without pH level adjustment. Reactions were carried out under nitrogen atmosphere using standard Schlenk techniques. CHN Analysis was performed on a Thermo EA1112 Flash CHNS-O Analyzer using standard microanalytical procedures. Palladium content was determined on a Perkin Elmer ICP-MS NexION 2000 using a Perkin Elmer Microwave Titan for digestion of powdered samples in conc. nitric acid. Transmission FT-IR spectra were recorded on a Bruker Alpha at room temperature using an ATR diamond sample tip. Thermogravimetric analysis was performed on a Q500 TGA by heating (20°C min^{-1}) samples under air (25 mL min^{-1}) in open platinum pans up to 1000 °C. The UV-visible absorption spectra were recorded on a Shimadzu UV-2550 UV-vis spectrometer as powders in the solid-state. The fluorescence spectra of the polymer powders were measured with a Shimadzu RF-5301PC fluorescence spectrometer at room temperature. Imaging of the polymer morphology was performed on a Hitachi S4800 Cold Field Emission SEM, with secondary electron, backscatter and transmission detectors. EDX Measurements were performed on an Oxford Instruments INCA ENERGY 250 M/X. PXRD Measurements were performed on a PANalytical X'Pert PRO MPD, with a Cu X-ray source, used in high throughput transmission mode with Kα focusing mirror and PIXCEL 1D detector. Time-correlated single photon counting experiments (TCSPC) were performed on an Edinburgh Instruments LS980-D2S2-STM spectrometer equipped with picosecond pulsed LED excitation sources and a R928 detector, with a stop count rate below 3%. A 371.5 nm laser diode (instrument response 100 ps fwhm) was used. Suspensions were prepared by ultrasonicating the polymers in water (concentration is the same as used in the corresponding TA experiments). The instrument response was measured with colloidal silica (LUDOX® HS-40, Sigma-Aldrich) at the excitation wavelength and decay times were fitted in Fluoracle software, based on suggested lifetime estimates and pre-exponential factors.

Hydrogen evolution experiments:

A screw-top vial was charged with the polymer powder (*ca.* 1 mg mL^{-1}) and a mixture of water/triethylamine/MeOH (1:1:1; 10 mL) and ultrasonicated until the photocatalyst was dispersed (30 min). The suspension was transferred into a quartz cuvette (2 × 4 × 1 cm, w × h × d), sealed with a septum and degassed by N_2 bubbling for 30 min. The reaction mixture was illuminated with a 300 W Newport Xe light-source (Model: 6258, Ozone free) for the time specified using appropriate filters. Gas samples were taken with a gas-tight syringe, and run on a Bruker 450-GC gas chromatograph equipped with a Molecular Sieve 13X 60-80 mesh 1.5 m × ⅛" × 2 mm ss column at 50°C with an argon flow of 40.0 mL min^{-1}. Hydrogen was detected with a thermal conductivity detector referencing against standard gas with a known concentration of hydrogen. Hydrogen dissolved in the reaction mixture was not measured and the pressure increase generated by the evolved hydrogen was neglected in the calculations. The rates were determined from a linear regression fit (see Section 8 for fits) and the error is given as the standard deviation of the amount of hydrogen evolved. No hydrogen evolution was observed for a mixture of water/methanol/trimethylamine under λ >295 nm illumination in absence of a photocatalyst.

Synthesis of **cLiP1**:[2]

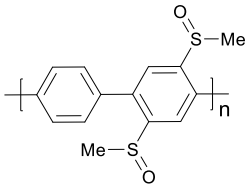

1,4-Dibromo-2,5-bis-(methylsulfinyl)benzene (1.00 g, 2.78 mmol), 1,4-phenylene bis(pinacol boronate) (918 mg, 2.78 mmol), $NaHCO_3$ (1.70 g, 42 mmol), $NaHCO_3$ aqueous solution (saturated, 4.5 mL), 1,2-dimethoxyethane (10 mL), and $[Pd(PPh_3)_4]$ (324 mg, 0.28 mmol) were combined in a three-necked round-bottom flask (50 mL). The solution was degassed by bubbling nitrogen through (5 min), and then the reaction mixture was heated to 90 °C and stirred for 24 h. After cooling to room temperature, H_2O (250 mL) was added and the solution was extracted with chloroform (3 × 250 mL). The organic layer was dried over anhydrous Na_2SO_4, filtered and evaporated to dryness. The crude oligomer was purified by precipitation into methanol (600 mL) from hot $CHCl_3$ solution (200 mL). After drying in a vacuum overnight at room temperature, the oligomer **cLiP1** was obtained as an off-white powder (412 mg, 54 %).

Anal. Calcd for $(C_{14}H_{12}O_2S_2)_n$: C, 60.84; H, 4.38%; Found C, 53.15; H, 4.15%.

Synthesis of **cLaP1**:[2]

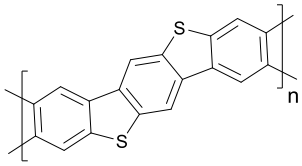

Oligomer **cLiP1** (400 mg) was added to cold trifluoromethanesulfonic acid (40 mL) in a round-bottom flask (100 mL) and stirred at room temperature for 22 h. The mixture was added to cold water (500 mL) with vigorous stirring to precipitate the product. The precipitate was filtered and washed with water several times. The methylated oligomer **cLaP1$^+$-Me** (336 mg) was obtained as a light brown powder, after drying in a vacuum overnight at room temperature.

The methylated oligomer **cLaP1$^+$-Me** (336 mg) was dissolved in a mixture of acetone/acetonitrile (80 mL, 1:1) at room temperature. Tetraethylammonium bromide (1.30 g) dissolved in an acetonitrile (10 mL) and water (2 mL) mixture was added to the oligomer **cLaP1$^+$-Me** solution and stirred vigorously at room temperature for 18 h. The yellow solid oligomer **cLaP1$^+$-Me** (223 mg), which precipitated as the result of demethylation, was collected by filtration, washed with water, and dried overnight at room temperature.

Oligomer **cLaP1$^+$-Me** (223 mg) was added to cold trifluoromethanesulfonic acid (15 mL) in a round-bottom flask and the reaction mixture was stirred at room temperature for 21 h. The reaction solution was poured into cold water (300 mL) with vigorous stirring to precipitate the product. The precipitate was filtered and washed with water several times. Oligomer **cLaP1** was obtained as a brown powder (222 mg, 65%), after drying in a vacuum overnight at room temperature.

Anal. Calcd for $(C_{12}H_4S_2)_n$: C, 67.90; H, 1.90%; Found C, 48.35; H, 2.76%.

Synthesis of **cLaP2**:[3]

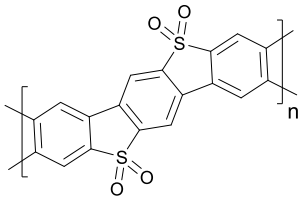

Oligomer **cLaP1**(100 mg) was dissolved in acetic acid (glacial, 5 mL) and heated to reflux (approx. 130 °C). Hydrogen peroxide solution (aqueous, 30 wt. %, 0.5 mL) was added dropwise and the reaction mixture was heated under reflux for 4 h. The reaction mixture was cooled down to room temperature and poured into cold DI water (50 mL). The precipitate was collected and washed with DI water. The product **cLaP2** (93 mg, 79%) was dried at room temperature *in vacuo* overnight.

Anal. Calcd for $(C_{12}H_4O_4S_2)_n$: C, 52.17; H, 1.46%; Found C, 45.46; H, 2.61%.

Synthesis of 3,7-bis(4,4,5,5-tetramethyl-1,3,2-dioxaborolan-2-yl)dibenzo[*b*,*d*]thiophene:[4]

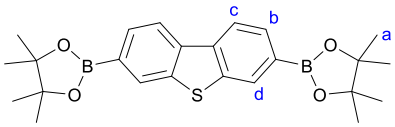

Under inert conditions, a flask was charged with 3,7-dibromodibenzo[*b,d*]thiophene (1 g, 2.9 mmol, 1 eq), B_2Pin_2 (1.6 g, 6.4 mmol, 2.2 eq.) and $[Pd(Cl)_2(dppf)_2]$ (64 mg, 3 mol%). Anhydrous DMSO (40 ml) and KOAc (1.7 g, 6 eq.) were added. The reaction mixture was heated to 80 °C for 28 hours. After cooling to room temperature, the mixture was poured onto ice and the precipitate was collected via filtration. The crude product was re-dissolved in ethyl acetate (120 ml) and filtered through a celite pad. The solvent was removed under reduced pressure. The beige product (965.2 mg, 75%.) was dried *in vacuo* at 40 °C for 48 hours.

IR (ATR, cm^{-1}): $\tilde{\upsilon}$ = 3053 (w),2977 (m),2925 (w),1736 (w), 1591 (m), 1545 (w), 1472 (m), 1388 (s),1369 (s), 1344 (vs), 1269 (s),1255 (s),1209 (m), 1165 (m), 1135 (vs), 1094 (vs), 1067 (m), 966 (s), 859 (s), 840 (s), 817 (s), 721 (s), 664 (s), 643 (m), 577 (m), 522 (m), 414 (m).

^{1}H NMR (300 MHz, $CDCl_3$, 298 K): δ (ppm) = 8.34 (dd, J = 0.8, 0.3 Hz, 2H, H^d), 8.20 (dd, J = 7.9, 0.3 Hz, 2H, H^c), 7.88 (dd, J = 7.9, 0.8 Hz, 2H, H^b), 1.39 (s, 24H, CH_3^a).

Synthesis of **P60**:[5]

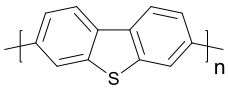

A flask was charged with 3,7-dibromodibenzo[*b,d*]thiophene (257 mg, 0.75 mmol), 3,7-bis-(4,4,5,5-tetramethyl-1,3,2-dioxaborolan-2-yl)dibenzo[*b,d*]thiophene (327 mg, 0.75 mmol), *N,N*-dimethylformamide (20 mL), an degassed, aqueous solution of K_2CO_3 (4 mL, 2.0 M), and $[Pd(PPh_3)_4]$ (15 mg, 2 mol%). After cooling to room temperature, the mixture was poured into water (150 mL). The precipitate was collected by filtration and washed with H_2O (50 mL) and methanol (100 mL). The crude product was purified by Soxhlet extraction with chloroform for 22 h. The beige product (236 mg, 86%) was collected and dried *in vacuo* at 80°C overnight.

Anal. Calcd for $(C_{24}H_{12}S_2)_n$: C, 79.09; H, 3.32%; Found C, 71.42; H, 3.45%.

2 UV-Vis and Photoluminescence Spectra

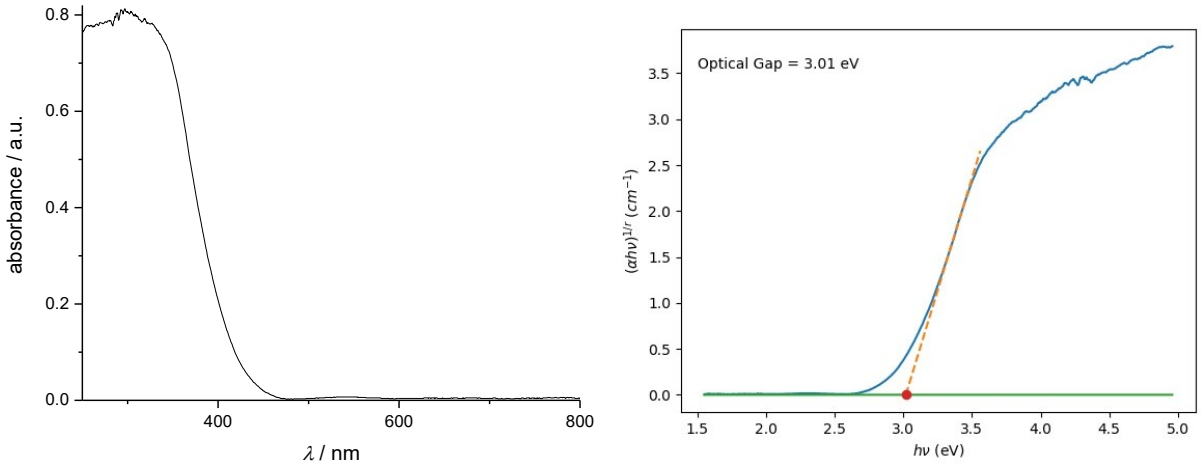

Figure S1. Solid-state UV-vis spectrum (left) and Tauc plot[6,7] with estimated optical gap (right) for ***cLiP1****.*

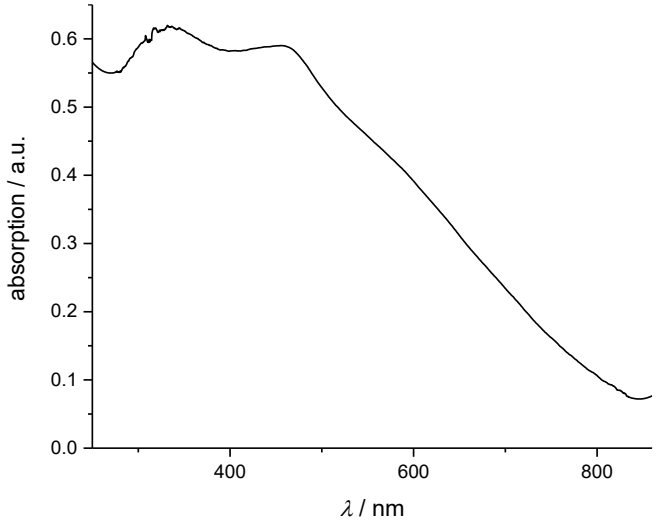

Figure S2. Solid-state UV-vis spectrum for ***cLaP1⁺-Me****.*

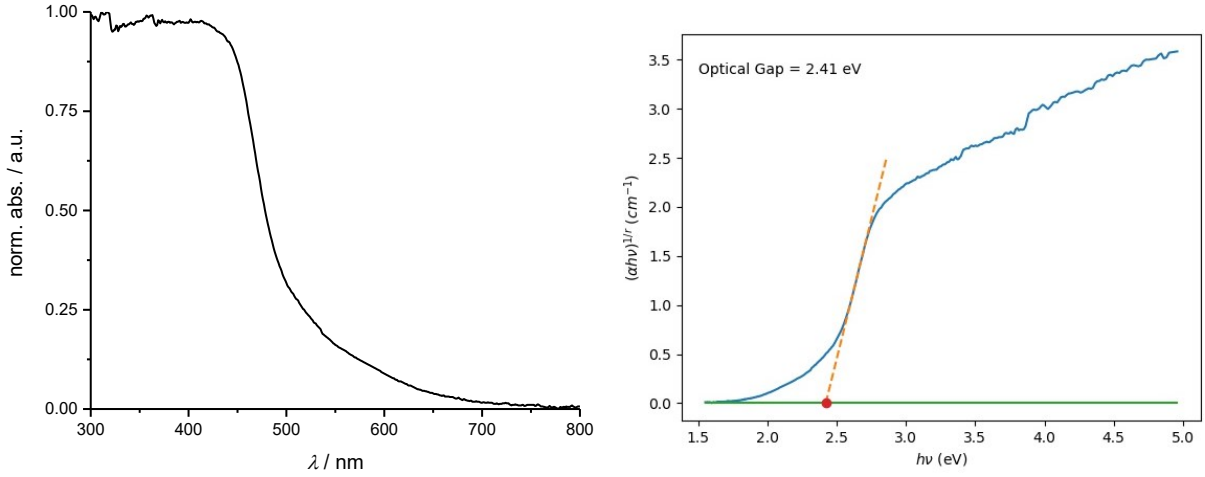

Figure S3. Solid-state UV-vis spectrum (left) and Tauc plot[6,7] with estimated optical gap (right) for ***cLaP1****.*

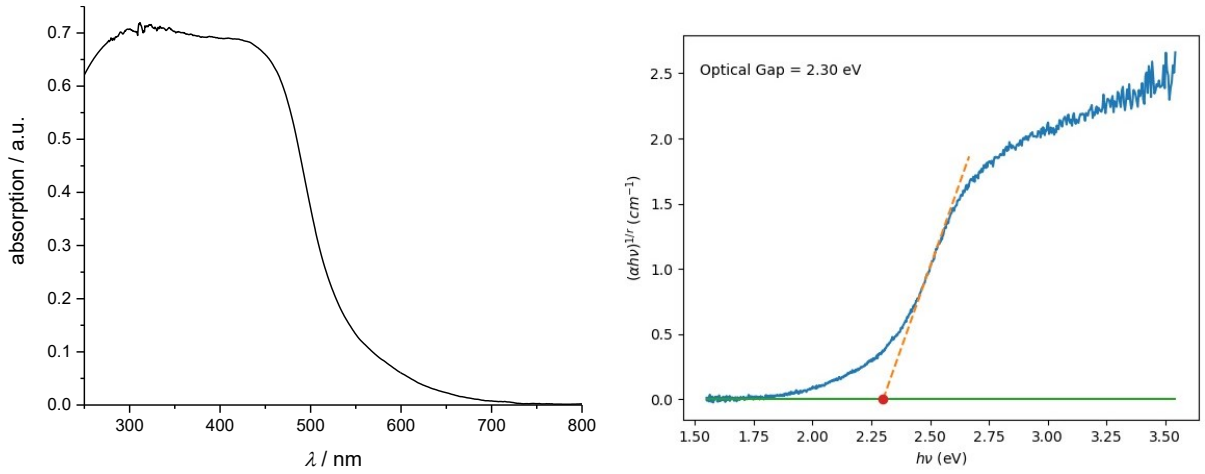

Figure S4. Solid-state UV-vis spectrum (left) and Tauc plot with estimated optical gap (right) for ***cLaP2****.*

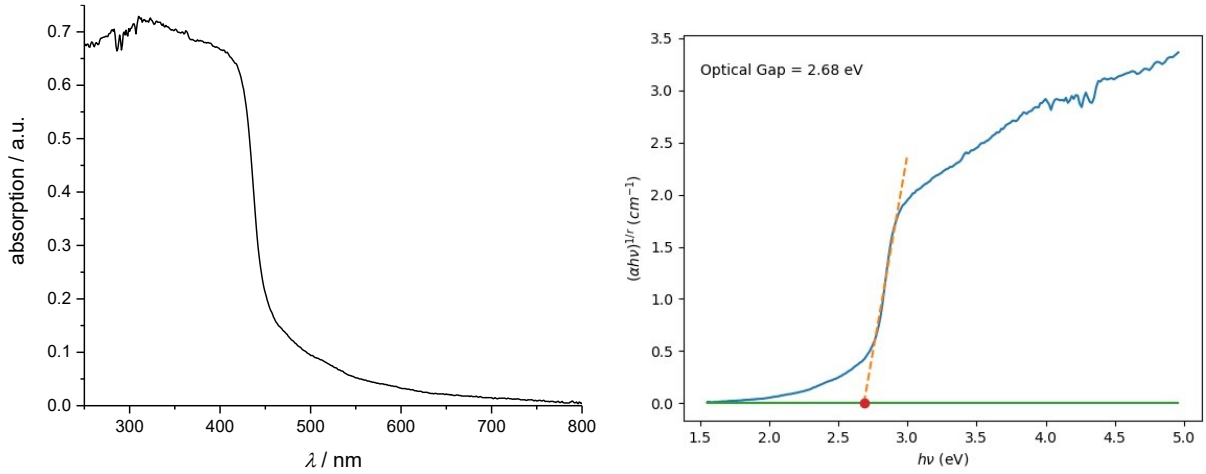

Figure S5. Solid-state UV-vis spectrum (left) and Tauc plot with estimated optical gap (right) for ***P60****.*

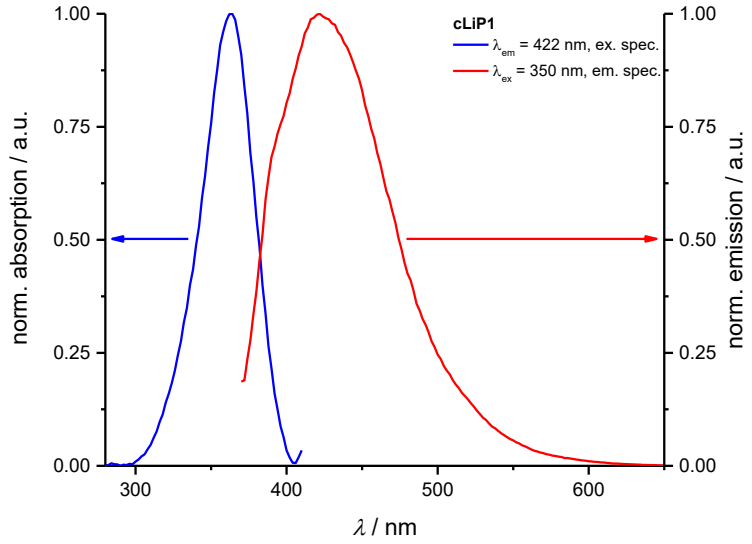

Figure S6. Excitation and emission spectra for ***cLiP1****.*

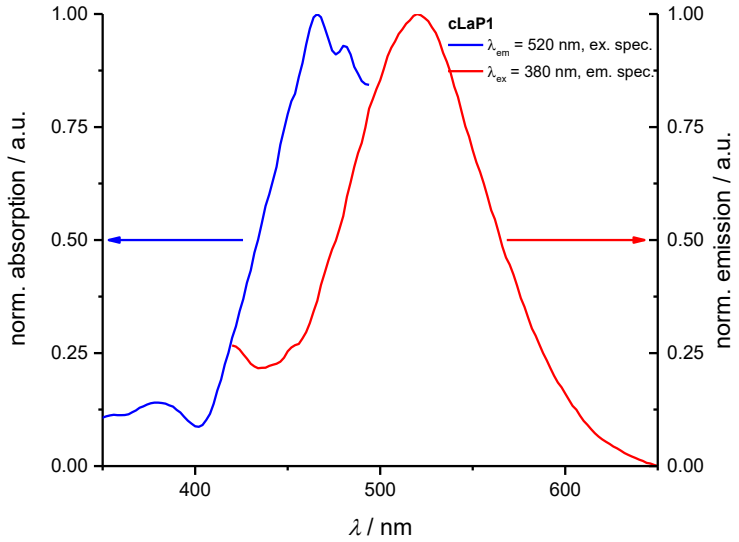

*Figure S7.Excitation and emission spectra for **cLaP1**.*

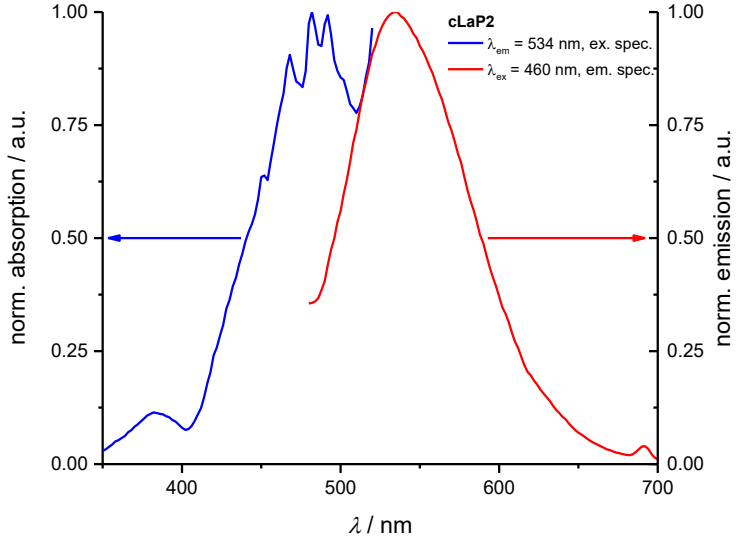

*Figure S8. Excitation and emission spectra for **cLaP2**.*

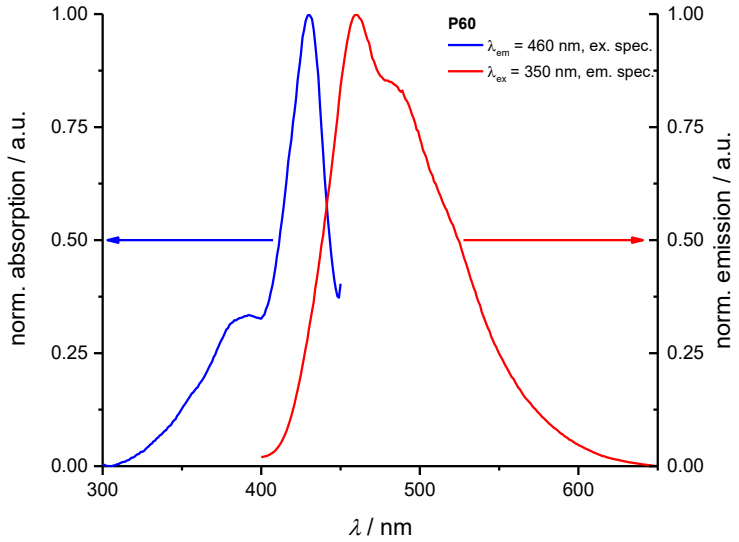

*Figure S 9. Excitation and emission spectra for **P60**.*

3 ATR-FT Infrared Spectroscopy

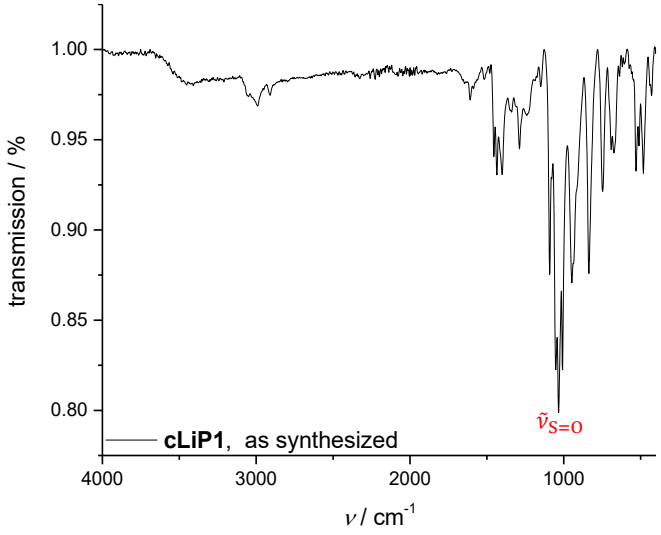

*Figure S10. ATR FTIR spectrum for **cLiP1** as synthesized with assignment of most prominent bands.*

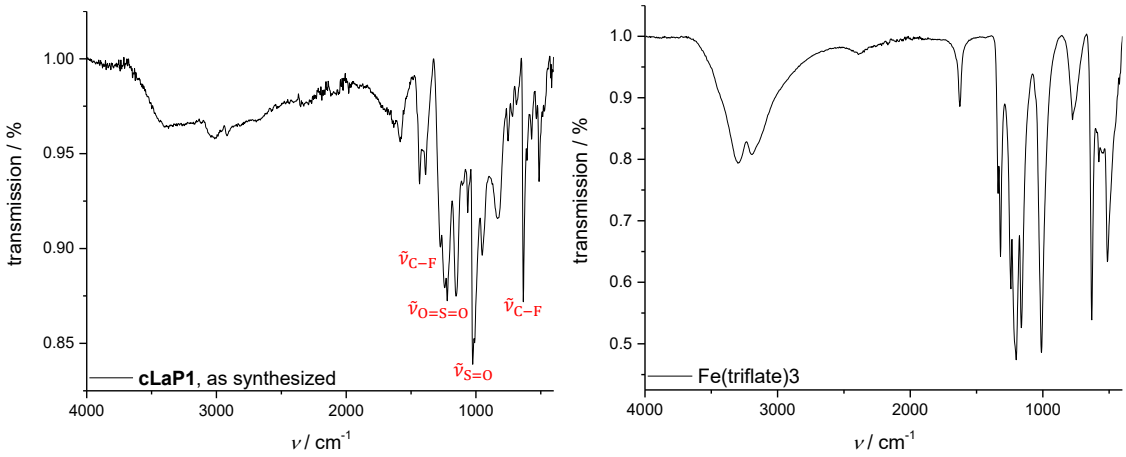

*Figure S11. ATR FTIR spectrum for **cLaP1** (left) as synthesized with assignment of most prominent bands and ATR FTIR spectrum for Fe(triflate)$_3$ for comparison (right).*

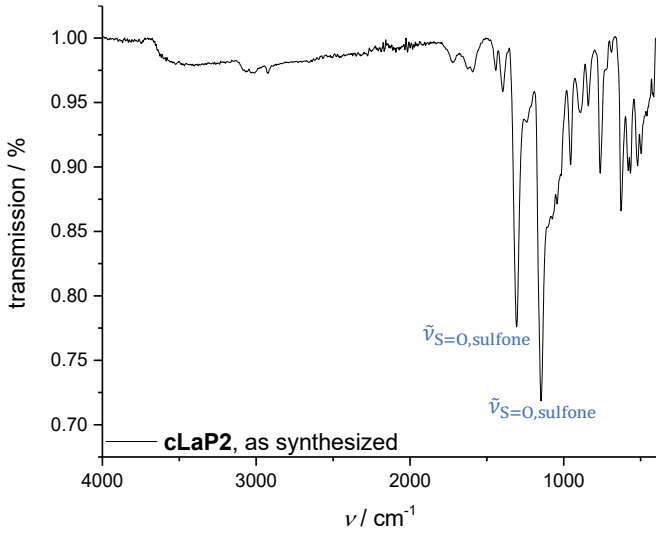

*Figure S12. ATR FTIR spectrum for **cLiP2** as synthesized with assignment of most prominent bands.*

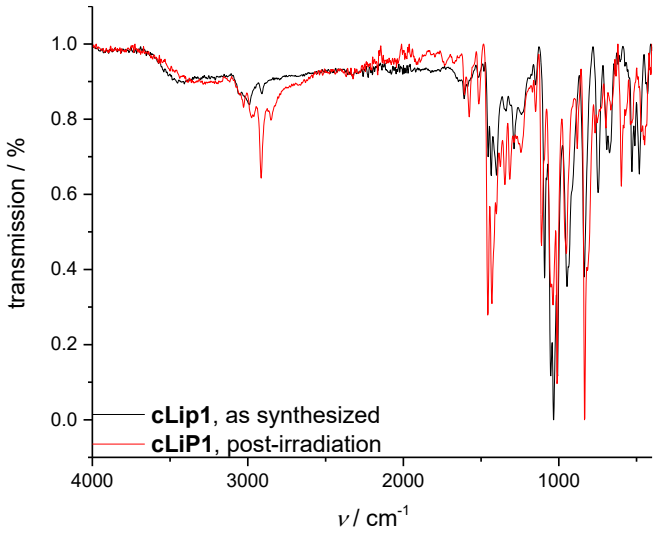

*Figure S13. ATR FTIR spectrum comparison for **cLiP1** as synthesized (black) and recovered after catalysis (red).*

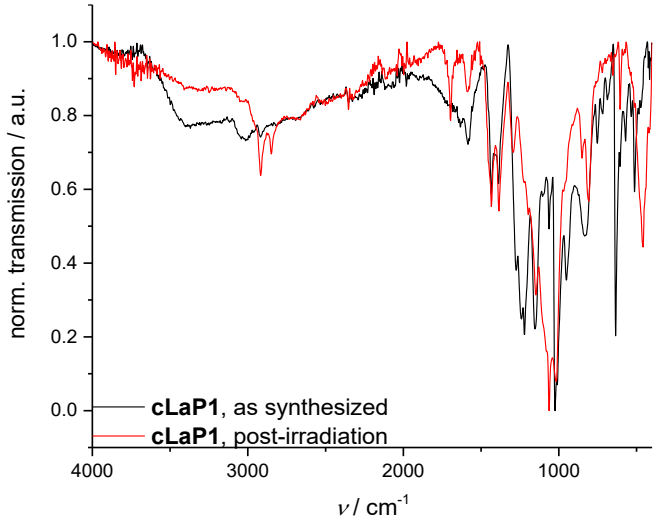

*Figure S14. ATR FTIR spectrum comparison for **cLaP1** as synthesized (black) and recovered after catalysis (red).*

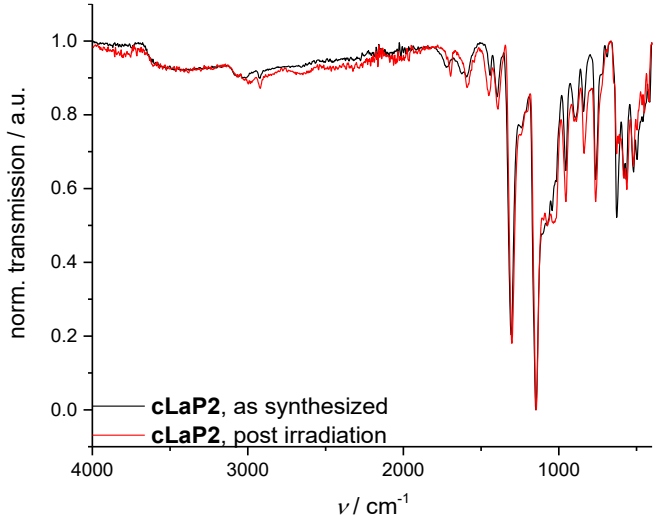

*Figure S15. ATR FTIR spectrum comparison for **cLaP2** as synthesized (black) and recovered after catalysis (red).*

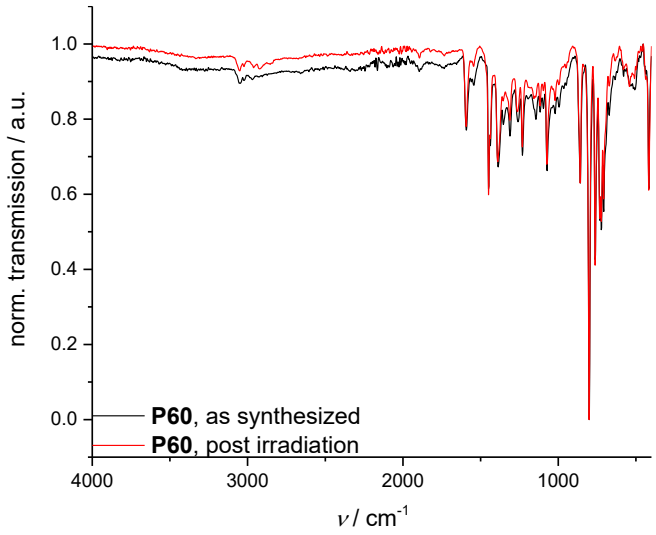

*Figure S16. ATR FTIR spectrum comparison for **P60** as synthesized (black) and recovered after catalysis (red).*

4 Powder X-Ray Diffraction

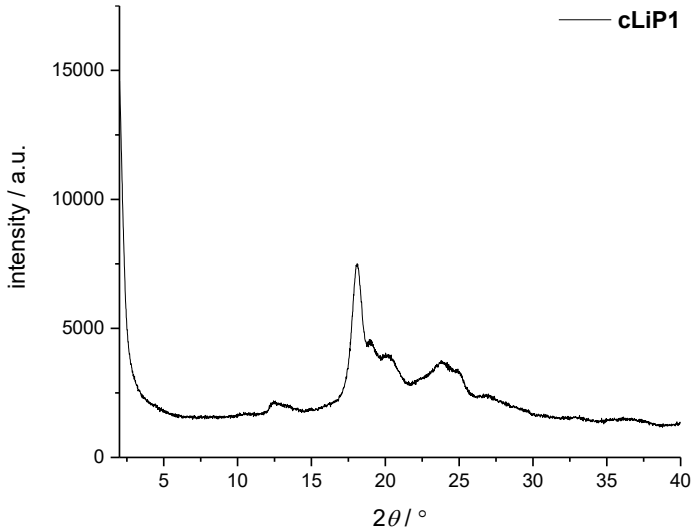

*Figure S17. PXRD pattern of **cLiP1**.*

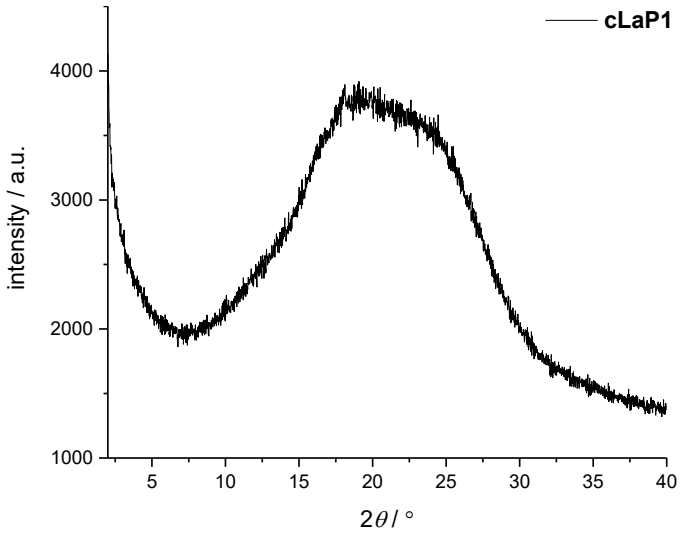

*Figure S18. PXRD pattern of **cLaP1**.*

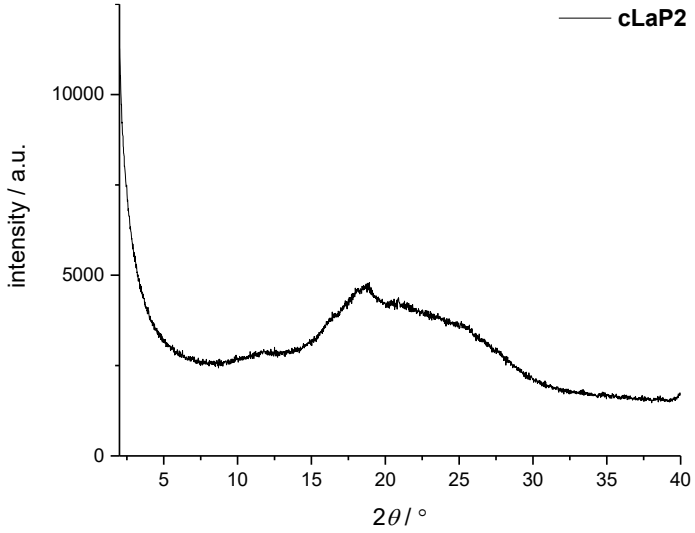

*Figure S19. PXRD pattern of **cLaP2**.*

5 Thermogravimetric Analysis

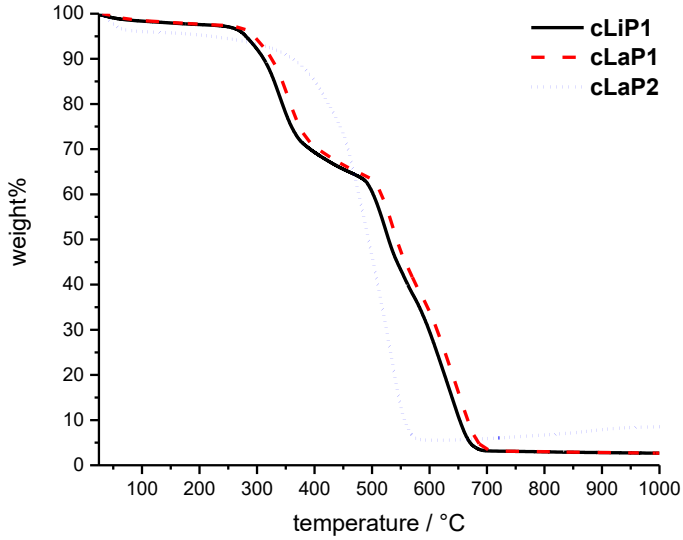

*Figure S20.TGA traces for **cLiP1**, **cLaP1** and **cLaP2**.*

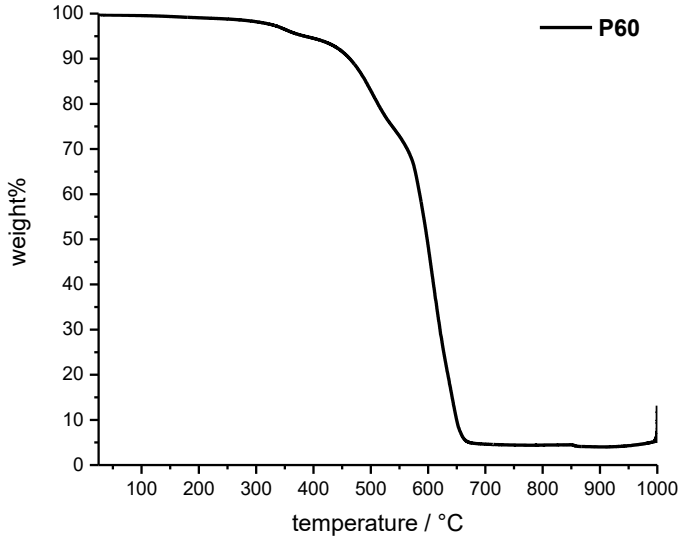

*Figure S21. TGA trace for **P60**.*

6 Scanning Electron Microscope/Energy-dispersive X-ray spectroscopy

cLiP1

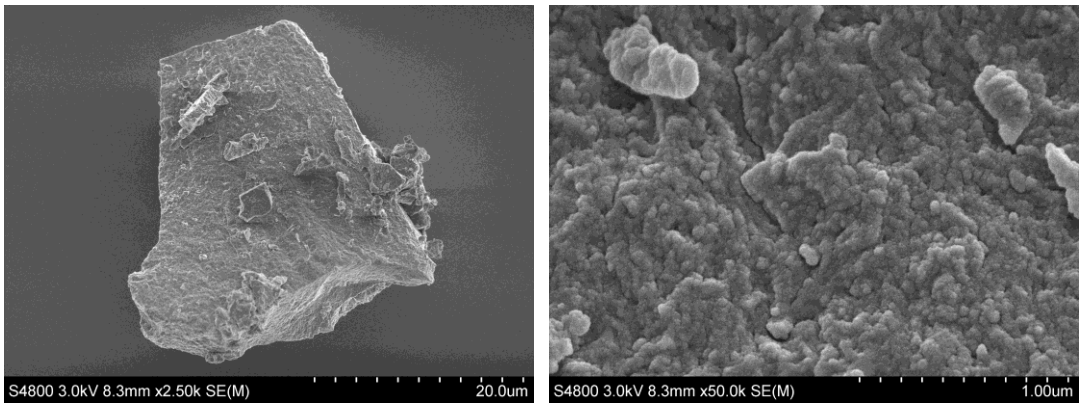

cLaP1

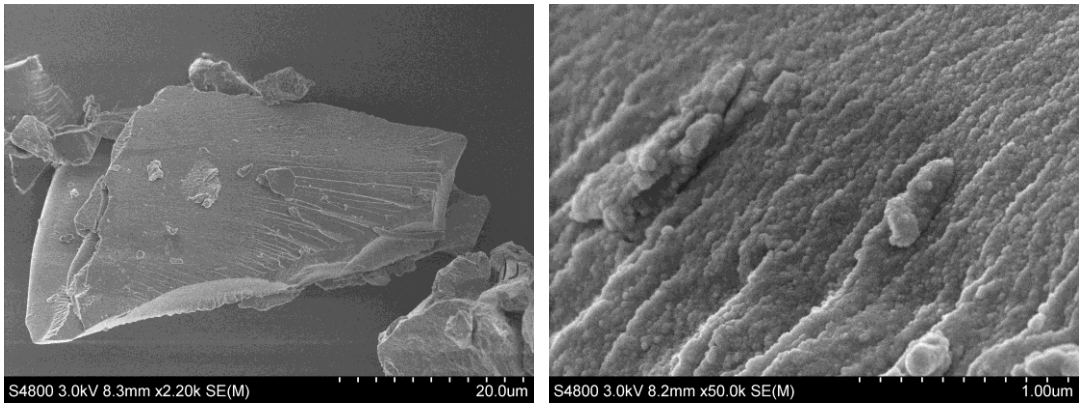

cLaP2

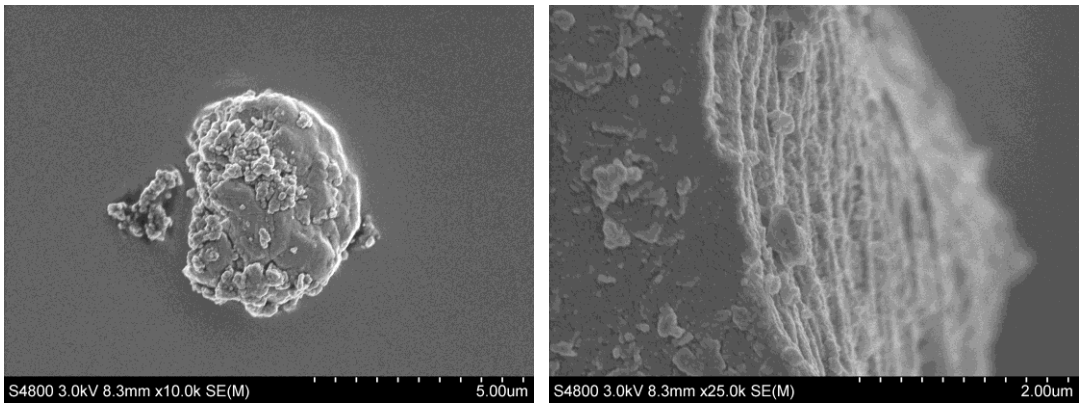

*Figure S22. SEM images for **cLiP1**, **cLaP1** and **cLaP2**.*

Table S1. Energy-dispersive X-ray spectroscopy. Average apparent composition of the sample determined via energy-dispersive X-ray spectroscopy in at least two points of the sample.

Element	cLiP1 / avg. wt. %	cLaP1 / avg. wt. %	cLaP2 / avg. wt. %
C	50.39	34.25	35.52
S	19.13	35.21	25.57
O	23.14	17.72	31.97
Br	5.33	7.85	4.87
Pd	0.88	0.79	0.42
P	0.62	0.78	0.63

7 ICP-MS Measurements

Table S2. Average palladium content in samples.

Sample	wt. %
P60	0.49
cLiP1	0.83
cLaP1	0.38
cLaP2	0.36

8 Hydrogen Evolution Experiments for Polymers

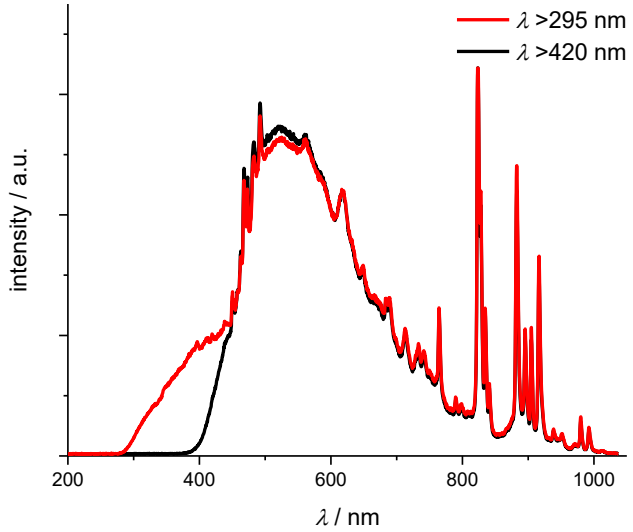

Figure S23. Output profile of the 300 W Xe-lamp equipped with a >295 nm (red) or a >420 nm (black) filter.

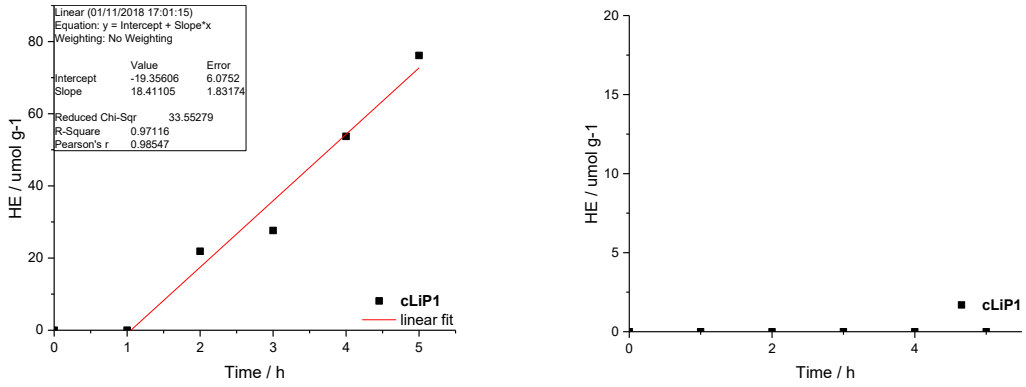

*Figure S24. Hydrogen evolution of **cLiP1** from a triethylamine/water/methanol mixture under λ >295 nm (left) and λ >420 nm (right) irradiation.*

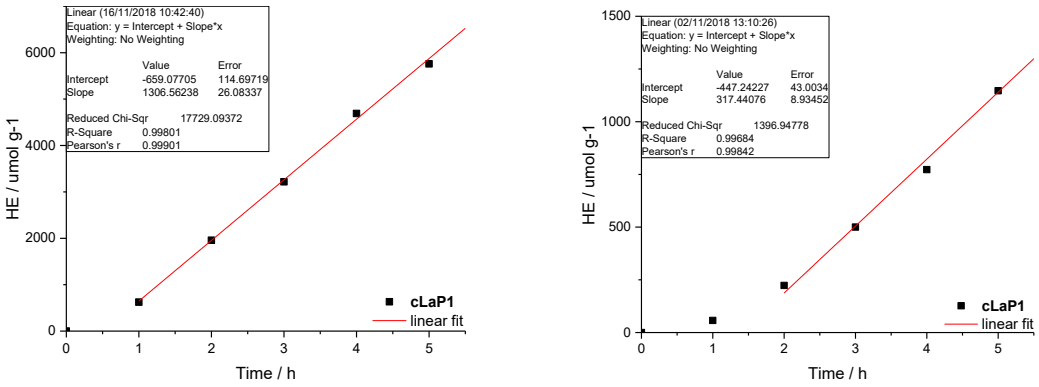

*Figure S25. Hydrogen evolution of **cLaP1** from a triethylamine/water/methanol mixture under λ >295 nm (left) and λ >420 nm (right) irradiation.*

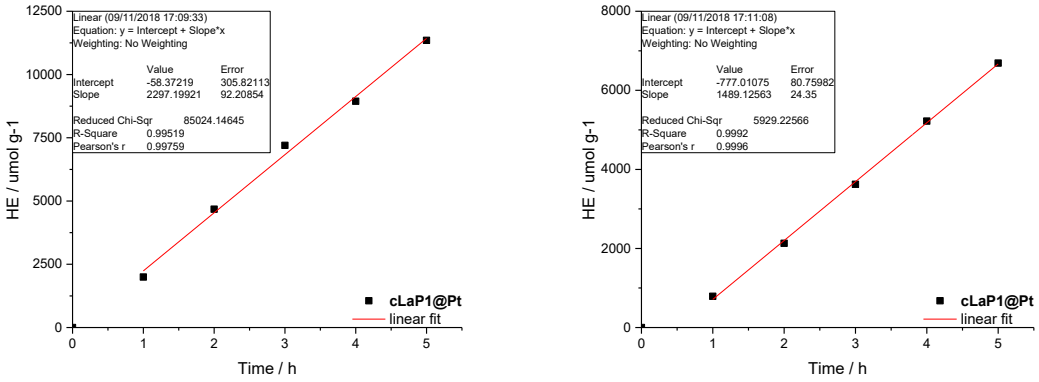

*Figure S26. Hydrogen evolution of **cLiP1@Pt** from a triethylamine/water/methanol mixture under λ >295 nm (left) and λ >420 nm (right) irradiation.*

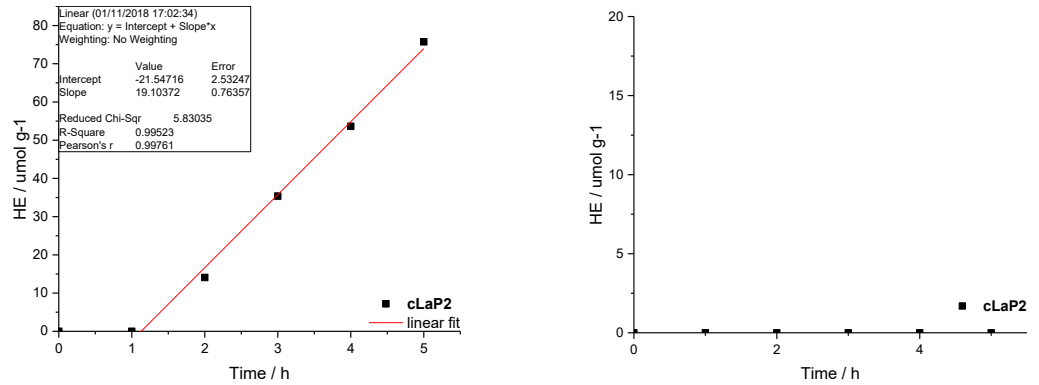

*Figure S27. Hydrogen evolution of **cLaP2** from a triethylamine/water/methanol mixture under λ >295 nm (left) and λ >420 nm (right) irradiation.*

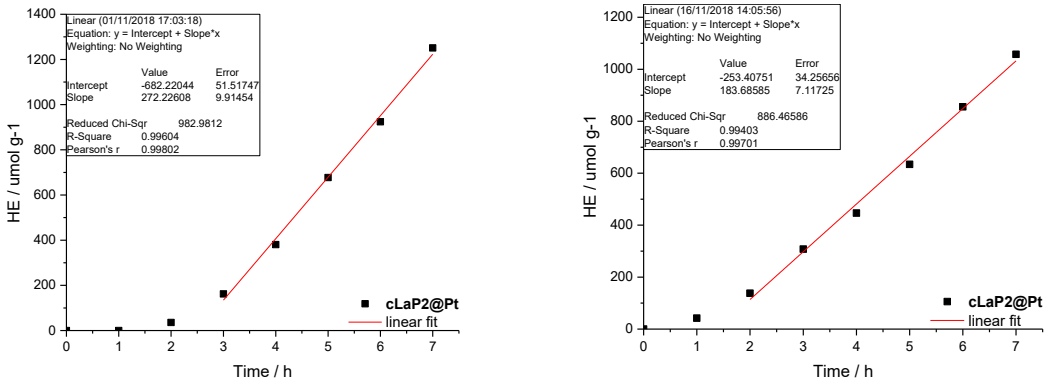

*Figure S28. Hydrogen evolution of **cLaP2@Pt** from a triethylamine/water/methanol mixture under λ >295 nm (left) and λ >420 nm (right) irradiation.*

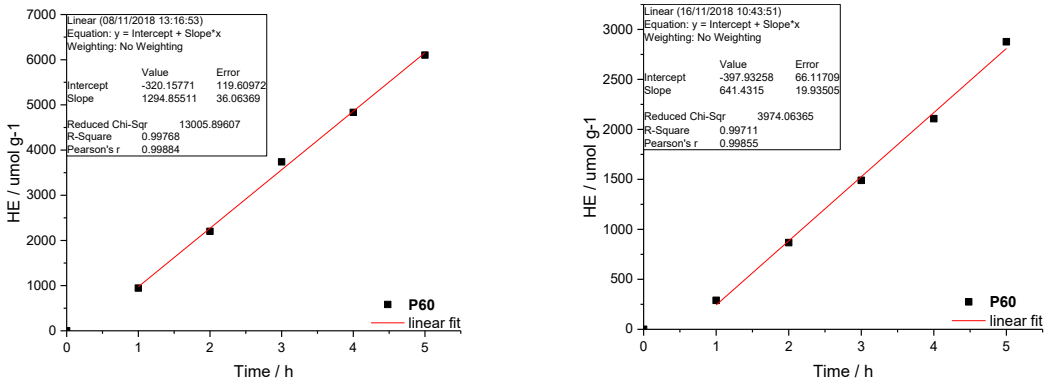

*Figure S29. Hydrogen evolution of **P60** from a triethylamine/water/methanol mixture under λ >295 nm (left) and λ >420 nm (right) irradiation.*

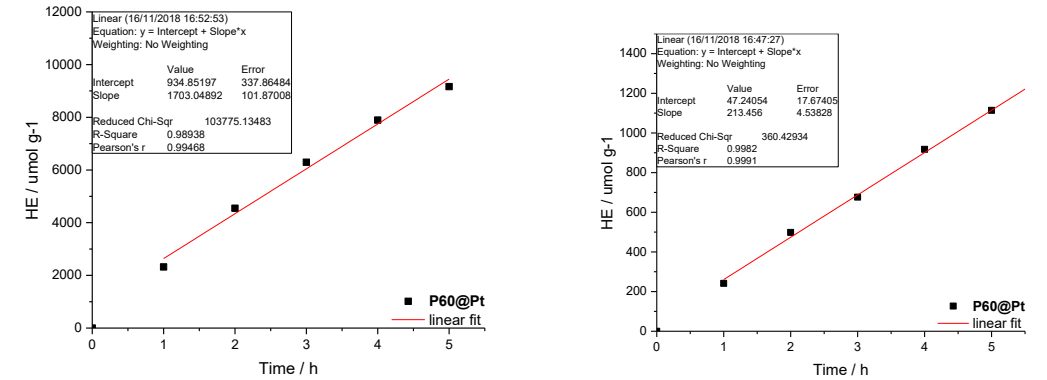

*Figure S30. Hydrogen evolution of **P60@Pt** from a triethylamine/water/methanol mixture under λ >295 nm (left) and λ >420 nm (right) irradiation.*

9 Stability Test for **cLaP1**

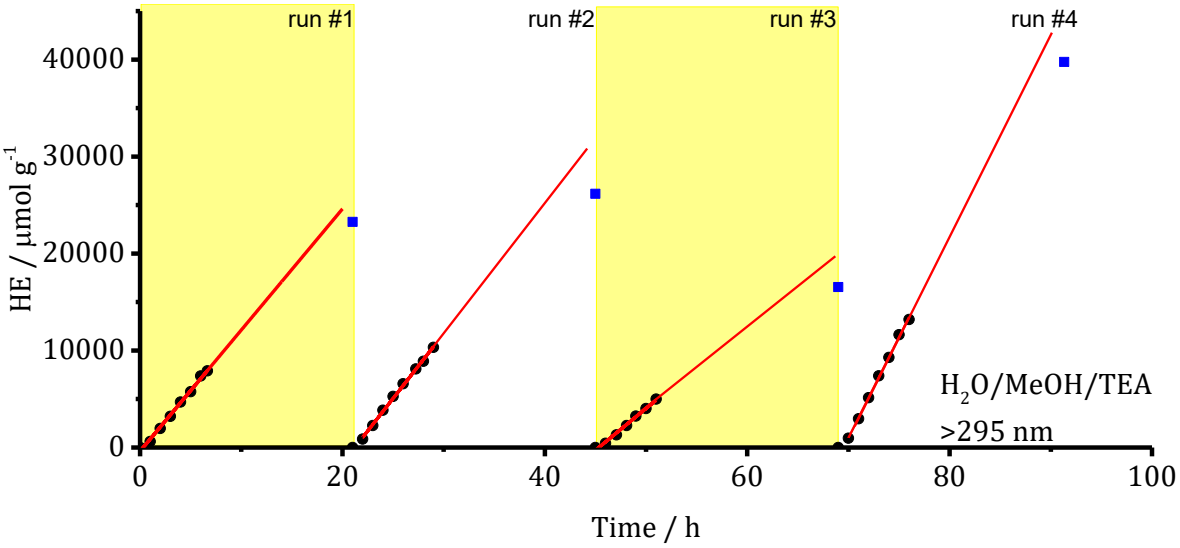

*Figure S31. Long-term catalytical run (90 hours) for **cLaP1**.*

	Irradiation conditions and sample treatment
run #1	8.3 mg, H2O/TEA/MeOH (1:1:1; 10 mL), degassed by bubbling N_2, >295 nm cut-off filter, 300 W Xe lamp; Sample was irradiated for 7 hours, samples of the gas phase were taken hourly (black circles) and the hydrogen evolution rate was estimated via a linear fit function (red line). Sample was left irradiated overnight. A final sample of the gas phase was taken the next morning (blue square) to ensure that hydrogen evolution had continued overnight. Slight deviation from the linear fit function is expected due to increase in pressure and possible leakage through the punctured septum. Estimated HER: 1307 ± 26 µmol h^{-1} g^{-1}
	Between run #1 and run #2, septum was exchanged and the sample was degassed.
run #2	sample from run #1, >295 nm cut-off filter, 300 W Xe lamp; Sample was irradiated for 8 hours, samples of the gas phase were taken hourly (black circles) and the hydrogen evolution rate was estimated via a linear fit function (red line). Sample was left irradiated overnight. A final sample of the gas phase was taken the next morning (blue square) to ensure that hydrogen evolution had continued overnight. Slight deviation from the linear fit function is expected due to increase in pressure and possible leakage through the punctured septum. Estimated HER: 1348 ± 34 µmol h^{-1} g^{-1}
	Between run #2 and #3, septum was exchanged and the sample was degassed.
run #3	sample from run #2, >295 nm cut-off filter, 300 W Xe lamp; Sample was irradiated for 6 hours, samples of the gas phase were taken hourly (black circles) and the hydrogen evolution rate was estimated via a linear fit function (red line). Sample was left irradiated overnight. A final sample of the gas phase was taken the next morning (blue square) to ensure that hydrogen evolution had continued overnight. Slight deviation from the linear fit function is expected due to

	increase in pressure and possible leakage through the punctured septum. A lower hydrogen evolution rate was estimated. We attribute this to an exhaustion of the sacrificial donor mixture and possible "poisoning" due to accumulation of byproducts. Estimated HER: 921 ± 17 µmol h^{-1} g^{-1}
	Between run #3 and #4, sample was recovered from the reaction mixture by centrifugation, removal of the supernatant, re-dispersion in H_2O (10 mL), repeated centrifugation and final filtration. Recovered **cLaP1** (5.0 mg) was dried *in vacuo*. A sample was taken for IR and UV-vis measurements at this point.
run #4	5.0 mg, H2O/TEA/MeOH (1:1:1; 10 mL), >295 nm cut-off filter, 300 W Xe lamp; Sample was irradiated for 7 hours, samples of the gas phase were taken hourly (black circles) and the hydrogen evolution rate was estimated via a linear fit function (red line). Sample was left irradiated overnight. A final sample of the gas phase was taken the next morning (blue square) to ensure that hydrogen evolution had continued overnight. Slight deviation from the linear fit function is expected due to increase in pressure and possible leakage through the punctured septum. A higher hydrogen evolution rate was estimated. We attribute this to a lower effective mass of the recovered **cLaP1** in comparison to still partially methylated initial catalyst as yielded from synthesis. Estimated HER: 2078 ± 34 µmol h^{-1} g^{-1}

10 Time-Correlated Single Photon Counting

Fluorescence life-times are obtained from fitting time-correlated single photon counting decays to a sum of three exponentials, which yield τ_1, τ_2 and τ_3, according to Equation 1.

Equation 1.Fitting function for time-correlated single photon counting decays.

$$\sum_{i=1}^{n} \left(A + B_i \, exp(-t/\tau_i)\right)$$

Weighted average lifetimes τ_{av} are calculated according to Equation 2.

Equation 2. Calculation of weighted average lifetime.

$$\sum_{i=1}^{n} B_i \tau_i$$

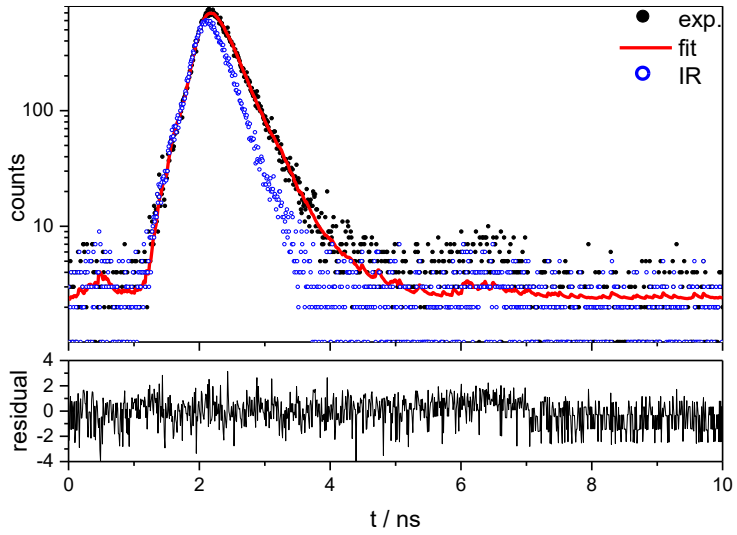

*Figure S32. Fluorescence life-time decay of **cLiP1** in aqueous suspension; instrument response (IR) shown in blue circles, experimental data in black dots and fitting function as a red line.*

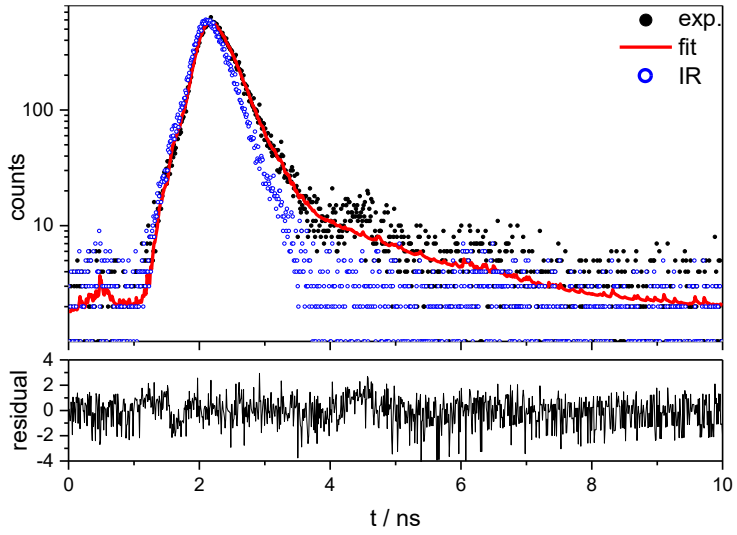

*Figure S33. Fluorescence life-time decay of **cLaP1** in aqueous suspension; instrument response (IR) shown in blue circles, experimental data in black dots and fitting function as a red line.*

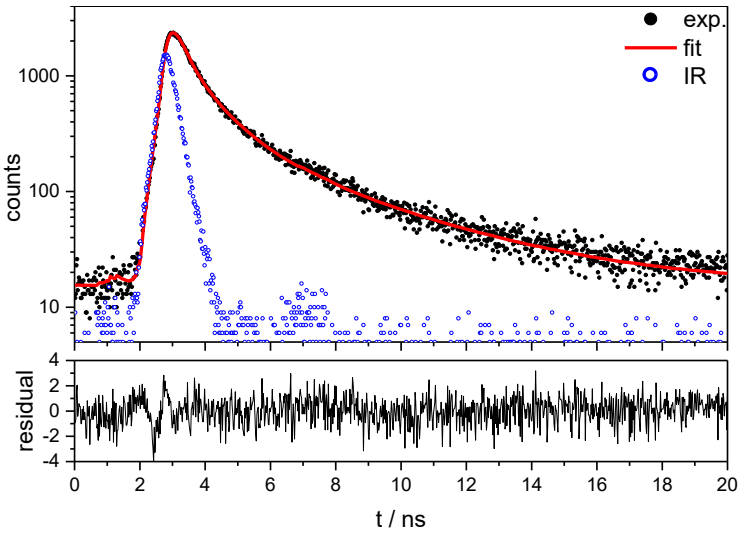

*Figure S34. Fluorescence life-time decay of **cLaP2** in aqueous suspension; instrument response (IR) shown in blue circles, experimental data in black dots and fitting function as a red line.*

Table S3.Overview of fitted and averaged fluorescence life-times in aqueous and H_2O/TEA/MeOH suspensions.

	solvent	λ_{em} / nm	τ_1 / ns	B1/ %	τ_2 / ns	B2/ %	τ_3 / ns	B3/ %	χ^2	τ_{avg} / ns
AV-6	H_2O	400	0.06	33.83	0.06	44.26	0.41	21.91	1.310	0.14
AV-7	H_2O	500	0.03	61.70	0.18	29.82	1.63	8.48	1.33	0.21
AV-20	H_2O	540	0.18	29.30	1.00	37.69	3.87	33.00	1.20	1.71

11 Transient Absorption Spectroscopy

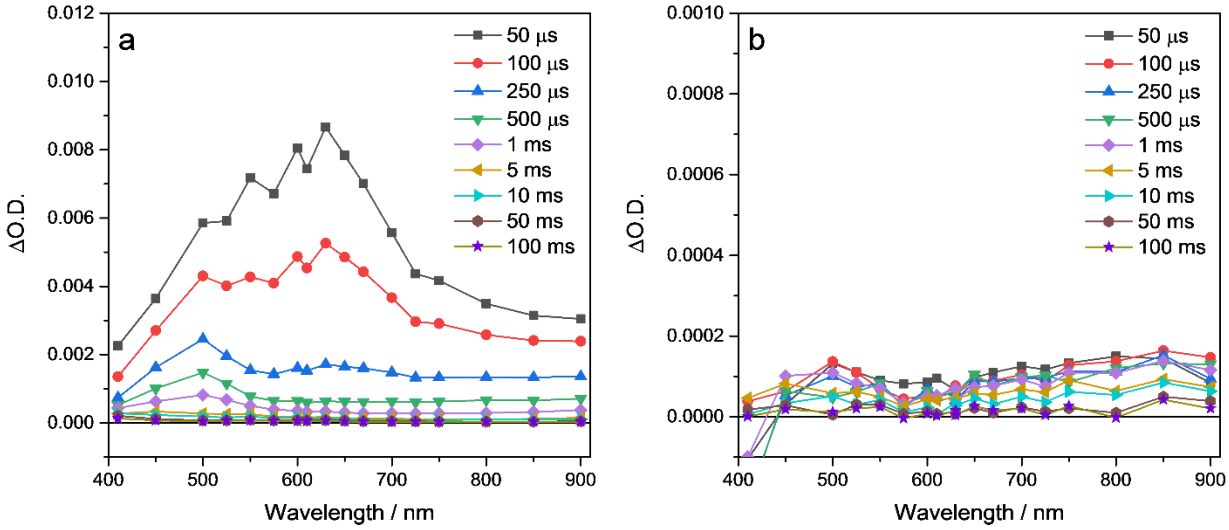

*Figure S35. µs-ms TA spectra of **cLaP1** suspended in a) H2O/TEA/MeOH and in b) H_2O which shows that the number of long-lived charges is greatly reduced in the absence of the mix system. TA spectra were recorded following excitation with a 355 nm (6 ns pulse) laser, under N_2.*

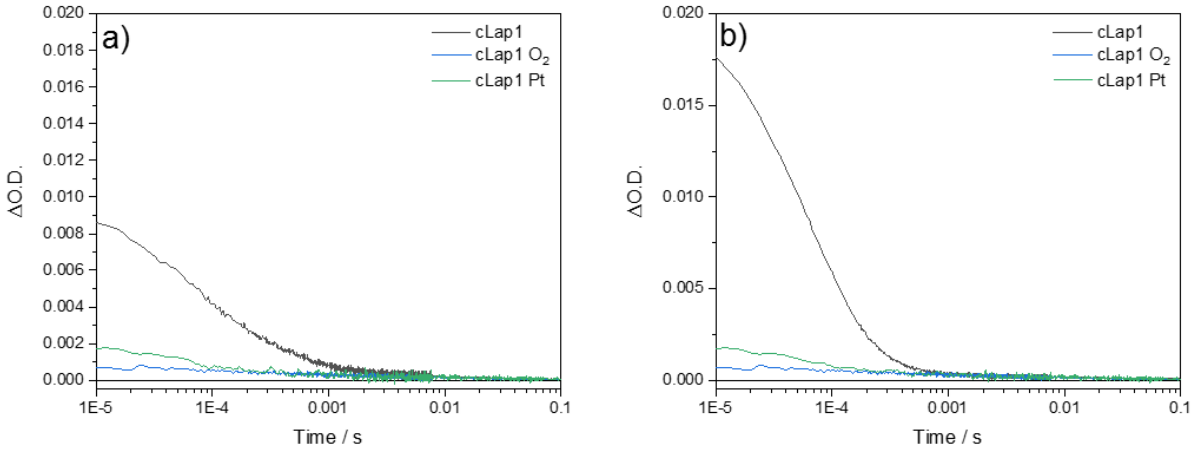

*Figure S36. µs-ms kinetic traces of **cLaP1** suspended in H2O/TEA/MeOH at probe wavelengths of a) 500 nm and b) 630 nm. TA spectra were recorded following excitation with a 355 nm laser (6 ns, 400 µJ cm⁻², 0.33 Hz), in N_2 (black), O_2 (blue) and with Pt in N_2 (green).*

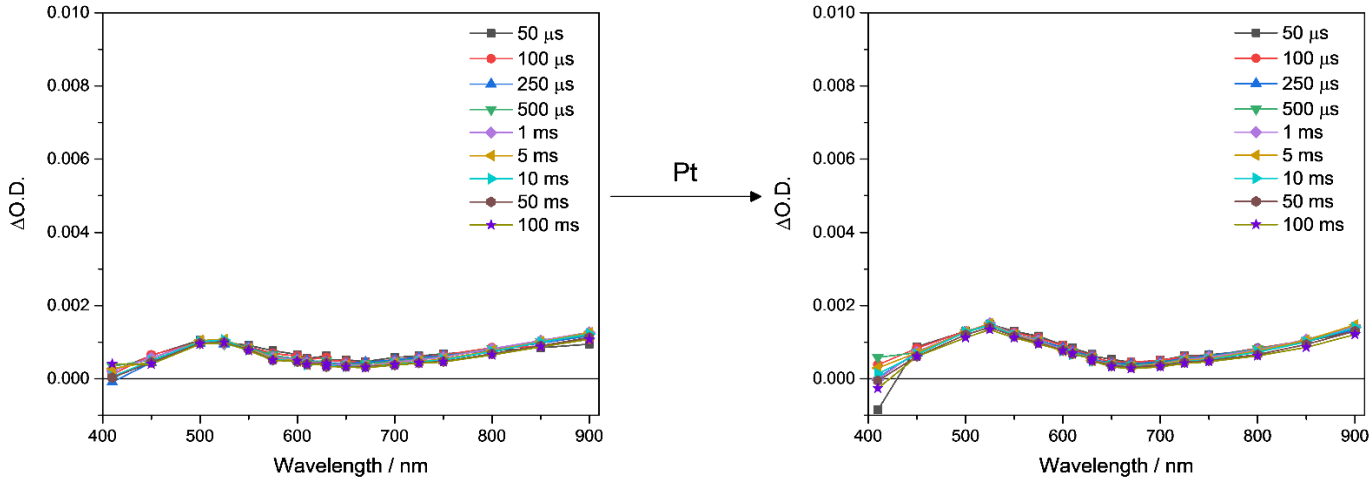

*Figure S 37. µs-ms TA spectra of **cLaP2** suspended in H_2O/TEA/MeOH before and after the addition of a Pt co-catalyst. TA spectra were recorded following excitation with a 355 nm laser (6 ns, 400 µJ cm⁻², 0.33 Hz), under N_2.*

12 (GFN/IPEA/sTDA)-xTB Calculations

All calculations were performed using the semi-empirical density functional tight-binding approach, xTB,[8] recently developed for the rapid calculation of geometries and optoelectronic properties of large molecular systems. The structural optimisation method (GFN-xTB[8]) is used to obtain optimized geometries from which ionisation potentials, electron affinities (obtained using IPEA-xTB[9]) and excitation energies (obtained with sTDA-xTB[10]) may be calculated. This latter method uses energy eigenvalues and wave functions obtained via xTB to calculate excited state properties. We have previously shown[11] that this semi-empirical approach, when a simple linear calibration procedure is performed using previously-obtained parameters,[11] produces absolute values of IP, EA and optical gap in excellent agreement with density functional theory.

For each polymer species (**cLaP1**, **cLaP2** & **cLiP1**), we calculate IP, EA and optical gaps for varying lengths of oligomer chains (defined by the number of aromatic rings along the polymer backbone). This is done to ensure that converged values are obtained across both ladder and non-ladder polymer species.

Table S4. Calculated optical gaps, Δ_o (lowest excitation of non-zero oscillator strength) for oligomer chains of length = 9, where 'length' is equal to the number of aromatic rings along the polymer backbone.

Polymer	Δ_o (eV)	Oscillator Strength (a.u.)
cLiP1	3.625	1.379
cLaP1	3.061	4.544
cLaP2	2.880	6.057

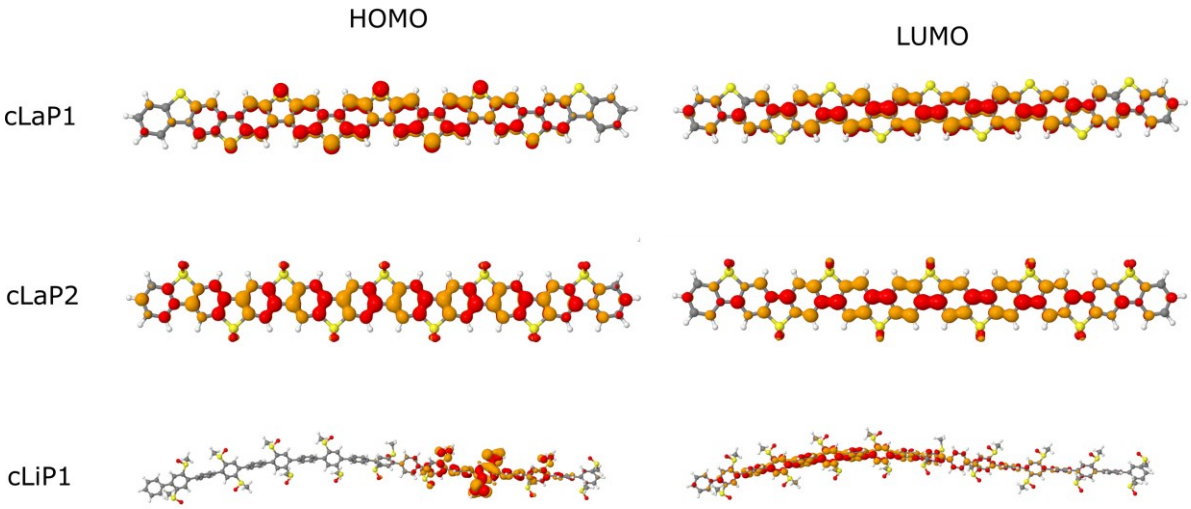

*Figure S38. Calculated HOMO and LUMO orbitals (isosurface value= 0.02) for **cLiP1**, **cLaP1** & **cLaP2**.*

13 References

1 P. Gao, X. Feng, X. Yang, V. Enkelmann, M. Baumgarten and K. Müllen, *J. Org. Chem.*, 2008, **73**, 9207–9213.

2 A. Haryono, K. Miyatake, J. Natori and E. Tsuchida, *Macromolecules*, 1999, **32**, 3146–3149.

3 a) K. Kawabata, M. Takeguchi and H. Goto, *Macromolecules*, 2013, **46**, 2078–2091; b) M. Maisuradze, G. Phalavadishvili, N. Gakhokidze, M. Matnadze, S. Tskhvitaia and E. Kalandia, *Int. J. Org. Chem.*, 2017, **07**, 34–41; c) H. Gilman and D. L. Esmay, *J. Am. Chem. Soc.*, 1952, **74**, 2021–2024;

4 T. Ishiyama, M. Murata and N. Miyaura, *J. Org. Chem.*, 1995, **60**, 7508–7510.

5 R. S. Sprick, B. Bonillo, R. Clowes, P. Guiglion, N. J. Brownbill, B. J. Slater, F. Blanc, M. A. Zwijnenburg, D. J. Adams and A. I. Cooper, *Angew. Chem. Int. Ed.*, 2016, **55**, 1792–1796.

6 J. Tauc, *Mater. Res. Bull.*, 1968, **3**, 37–46.

7 L. Wilbraham, *Code for Preparation of Tauc plots,* available at: https://github.com/ZwijnenburgGroup/taucauto.

8 S. Grimme, C. Bannwarth and P. Shushkov, *J. Chem. Theory Comput.*, 2017, **13**, 1989–2009.

9 V. Ásgeirsson, C. A. Bauer and S. Grimme, *Chem. Sci.*, 2017, **8**, 4879–4895.

10 S. Grimme and C. Bannwarth, *J. Chem. Phys.*, 2016, **145**, 54103.

11 L. Wilbraham, E. Berardo, L. Turcani, K. E. Jelfs and M. A. Zwijnenburg, *J. Chem. Inf. Model.*, 2018, Article ASAP, DOI: 10.1021/acs.jcim.8b00256.